The encoding of interoceptive-based predictions by the paraventricular nucleus of the thalamus D2+ neurons

Briana Machen[1], Sierra N. Miller[1], Al Xin[2], Carine Lampert[1], Lauren Assaf[1], Julia Tucker[1], Francisco Pereira[2], Gabriel Loewinger[2], Sofia Beas[1#]

1 – Department of Neurobiology, University of Alabama at Birmingham, Birmingham, AL, USA.

2 – Machine Learning Core, National Institute of Mental Health, Bethesda, MD, USA.

[#] Correspondence: Sofia Beas, Ph.D. Email: sbeas@uab.edu

ABSTRACT

Understanding how the brain integrates internal physiological states with external sensory cues to guide behavior is a fundamental question in neuroscience. This process relies on interoceptive predictions—internal models that anticipate changes in the body's physiological state based on sensory inputs and prior experiences. Despite recent advances in identifying the neural substrates of interoceptive predictions, the precise neuronal circuits involved remain elusive. In our study, we demonstrate that Dopamine 2 Receptor (D2+) expressing neurons in the paraventricular nucleus of the thalamus (PVT) play key roles in interoception and interoceptive predictions. Specifically, these neurons are engaged in behaviors leading to physiologically relevant outcomes, with their activity highly dependent on the interoceptive state of the mice and the expected outcome. Furthermore, we show that chronic inhibition of PVT^{D2+} neurons impairs the long-term performance of interoceptive-guided motivated behavior. Collectively, our findings provide insights into the role of PVT^{D2+} neurons in learning and updating state-dependent predictions, by integrating past experiences with current physiological conditions to optimize goal-directed behavior.

INTRODUCTION

All organisms perceive the world through their bodily senses. As such, understanding how the brain integrates internal physiological states with external sensory cues to guide behavior is a fundamental question in neuroscience. Although much is known about perception of external sensory cues, less is known about the mechanisms mediating the perception of internal bodily cues. Interoception is the ability to sense, track, and integrate signals originating from within the body, such as hunger, thirst, temperature, heart rate, and blood CO_2 levels, amongst others[1-5]. However, interoception plays a broader, more encompassing, role within the systems governing emotion, motivation, decision making, and social cognition[4,6,7]. Moreover, impairments in the ability to monitor bodily signals exist across many psychiatric illnesses, such as panic disorder, anxiety, depression, and substance use disorders[2,3,8].

Prevailing models of interoception posit that physiological signals are sensed, tracked, integrated, and prioritized to guide behaviors[1-6,8,9]. Studies on the mechanisms mediating interoception have largely focused on the “sensing” and “tracking” aspects. Indeed, hypothalamic areas, such as the arcuate nucleus (ARC) and the lateral hypothalamus (LH), as well as hindbrain areas, such as the medulla and nucleus of the solitary tract (NTS), play a distinctive role in detecting hunger signals from the body and the regulation of feeding behaviors[10,11]. Additional regions, such as the median preoptic nucleus (MnPO) and the subfornical organs (SFO), mediate thirst and water drinking behaviors[12-14]. However, much less is known about how the brain integrates these signals and prioritizes them to create the perception of internal states.

Once sensed, these peripheral physiological signals need to be integrated with sensory cues from the external environment, as well as learning from previous experiences, to create internal models[4,5,9]. These internal models help individuals anticipate changes in the body’s physiological state based on these factors (current physiological state, environmental cues, learned experiences) – a process known as interoceptive predictions[4,5,9]. These predictions allow the brain to prepare for and respond proactively to physiological demands, ensuring efficient and

adaptive regulation of bodily processes. These also represent a fundamental aspect of how the brain maintains homeostasis and guides behavior. By predicting physiological needs, the brain prioritizes behaviors that restore or preserve bodily balance to influence decisions and motivations. Despite the progress made in identifying the neural substrates of interoceptive predictions, the precise neuronal circuits involved in encoding these predictions remain poorly understood.

The paraventricular nucleus of the thalamus (PVT) has emerged as a critical node in the limbic system, yet its functional role remains unclear. Anatomical studies show that the PVT receives converging inputs from brain areas that process homeostatic and interoceptive signals[15-17]. Hypothalamic and brainstem areas that process physiological signals, such as hunger[11,18-20], thirst[12-14], thermoregulation[21,22], pain[23-25] , and stress[26-28] project to and recruit the PVT. Moreover, optogenetic activation of inputs to the PVT from hunger processing areas, such as the ARC and LH, result in feeding and food-seeking behaviors[18,20,29]; while stimulation from inputs originating in the MnPO result in water intake and seeking behavior[13,14]. These studies demonstrate that PVT neurons participate in interoception. In addition, the PVT receives signals about environmental cues from cortical areas, such as the medial prefrontal cortex (mPFC)[30-34]. The activity of PVT neurons is also altered by external cues when paired with physiologically relevant stimuli[18,27,30,32-36]. As such, the PVT is anatomically well-positioned to effectively bridge the interoceptive and exteroceptive domains to create internal states that guide behavior.

While commonly glutamatergic, PVT projection neurons are heterogeneous[26,37-39]. Particularly, our previous research found that a subtype of PVT neurons (PVT neurons expressing the dopamine receptor 2; PVT^{D2+}) are tuned to changes in current physiological states[26,39] and as such, play a more general role in integrating and encoding these states. In this study, we used fiber photometry to further investigate the *in vivo* dynamics of PVT^{D2+} neurons in mice performing a reward foraging task. Specifically, we focused on thoroughly characterizing the precise role these neurons play in interoceptive perception that influence goal-directed behaviors. We

discovered that PVT^{D2+} neurons integrate factors, such as physiological needs, environmental cues, and previous experiences to compute an interoceptive prediction. This prediction, in turn, guides motivated behavior. Moreover, we show that chronic chemogenetic inhibition of PVT^{D2+} neurons results in long-term deficits in interoceptive guided motivated behavior. Collectively, our results highlight the reconceptualization of PVT^{D2+} neurons as a neural mechanism that is critical for interoception and interoceptive predictions that are needed for the perception of internal states.

METHODS

Mice

All procedures were performed in accordance with the University of Alabama Birmingham *Institutional Animal Care and Use Committee (IACUC)* Guide for the Care and Use of Laboratory Animals. For this, female and male Drd2-Cre mice (GENSAT founder line ER44) were used. These mice were between 8 – 15 weeks of age and were group housed under a 12-h light-dark cycle (6 a.m. to 6 p.m. light), at a temperature of 70–74 °F and 40–65% humidity. After surgery, mice were single-housed and were provided with food and water *ad-libitum.* Two days before initiating behavioral training procedures, food was removed for food restriction and the amount of food provided was according to 85% of their free-feeding weight. Water was maintained *ad-libitum,* unless otherwise specified. Mice returned to ad-libitum feeding after testing.

Viral vectors

For GCaMP, we used AAV9-hSyn-FLEX-GCaMP6s-WPRE-SV40 which was produced by the Vector Core of the University of Pennsylvania. For our chemogenetic inhibition, we used AAV2-hSyn-DIO-hM4D(Gi)-mCherry which was produced by Addgene. For controls, we used AAV2-CAG-Flex-tdTomato which was produced by the vector core of the University of North Carolina.

100 **Drugs**

101 CNO (Enzo Life Sciences, catalog# BML-NS105) was used at a 10 mg/Kg dose.

102 **Stereotaxic surgery**

103 Mice were given viral injections (approximately 1 µl) at the following stereotaxic coordinates (at a
104 6°angle): pPVT, −1.60 mm from Bregma, 0.25 mm lateral from midline, and −3.35 mm vertical
105 from the cortical surface. Optical fibers with diameters of 400 µm (0.48 NA - Neurophotometrics)
106 were used. These fibers were implanted over the pPVT immediately following viral injections
107 (targeted 300-400 µm above the injection site). Following stereotaxic injections, animals were
108 allowed to recover for 2–3 weeks to ensure maximal AAV expression.

109 **Foraging-like reward-seeking task**

110 The foraging track consisted of a linear maze (81.28 × 21.59 × 29.21, L ×W× H in cm). The
111 Ethovision (Noldus) tracking system allowed us to track the movement of the mice through the
112 maze. The maze consisted of three zones: trigger zone, corridor, and reward zone. The opposite
113 ends of the track were designated as the trigger zone and reward zone and were connected by a
114 long corridor. The task consisted of 60 min-long sessions of self-paced trials and mice received
115 one test session per day. For each trial, food-restricted mice were trained to wait in the trigger
116 zone for two seconds. An LED mounted on top of the reward magazine port was then illuminated,
117 which signaled reward availability, allowing mice to run from the trigger zone down the corridor
118 and into the reward zone to retrieve a food reward. The strawberry milkshake (SMS) reward
119 consisted of strawberry Ensure® mixed with 20% sucrose water. The non-caloric reward
120 consisted of 10% sucralose (Splenda®) solution. The sucrose reward consisted of 10% sucrose
121 solution. Reward delivery and food consumption signaled trial termination, and therefore mice

122 had to return to the trigger zone to initiate another trial. Experimental schedule and data
123 acquisition were implemented through the Ethovision software for operant control.

124 **Four-bottle choice assessment**

125 Mice were individually housed and tested in their home cages. After becoming accustomed to
126 each solution, hungry mice were given free access to four bottles in their home cage. Each bottle
127 contained one of the following: water, a 10% sucrose solution, a non-caloric 10% sucralose
128 solution, or a strawberry milkshake (strawberry Ensure® mixed with 20% sucrose water). After a
129 2-hour testing period, the total volume consumed (in mL) for each solution was recorded.
130 Consumption was averaged across two sessions. To prevent place preference, the placement of
131 the solutions in the cage was randomized across sessions.

132 **Bulk Ca^{2+} and fiber photometry**

133 All photometry experiments were performed using an RZ5P acquisition system (Tucker-Davis
134 Technologies; TDT) equipped with a real-time signal processor and controlled by a software
135 interface (Synapse version 92). Specifically, the system is integrated with two continuous
136 sinusoidally modulated LED at 473 nm (211 Hz) and 405 nm (531 Hz) that serves as the light
137 source to excite GCaMP6s and an isosbestic autofluorescence signal, respectively. The LED
138 intensity (ranging 10–15 μW) at the interface between the fiber tip and the animal was constant
139 throughout the session. Fluorescence signals were collected by the same fiber implant that was
140 coupled to a 400 μm optical patch-cord (0.48 NA) and focused onto two separate photoreceivers
141 (2151, Newport Corporation) connected to the emission ports of a custom-ordered fiber
142 photometry Mini Cube (Doric Lenses). TTL pulses recorded by the same system were used to
143 annotate the occurrence of behavioral manipulations. For the measurements of fluorescent
144 calcium signals and $\Delta F/F$ analysis, a least-squares linear fit to the 405 nm signal to align it to the

470 nm signal was first applied. The resulting fitted 405 nm signal was then used to normalize the 473 nm as follows: ΔF/F = (473 nm signal − fitted 405 nm signal)/fitted 405 nm signal. All GCaMP signal data is presented as the z-score of the dF/F from a baseline (2 seconds) prior to the onset of events.

In vivo data analysis

After calculating the z-score of the dF/F for each event in every trial the mice performed, the latency to the reward zone was calculated. All trials that took longer than 11 seconds and the events corresponding to that trial (decision to approach, approach, reward zone arrival, reward delivery) were excluded. Less than 10% of the trials met this exclusion criterion. After that, the trials and events for each individual test session were sorted by their trial order within a session. After sorting the trials in each test session, these were then divided into 5 equivalent trial blocks. This binning strategy allowed for comparable representation per animal in both block trials and was used by prior studies to test the effect of trial order [39] which permits the comparison of the activity dynamics of PVT neurons and how they were modulated by the motivational states of the mice across the progression of each test session.

FLMM - Trial order effects were also confirmed using a Functional Linear Mixed Model (FLMM). This analysis, previously described in detail[39-41], combines linear mixed models (LMM) and functional regression. The FLMM framework produces plots for each covariate in the model (e.g., trial order effects) to show whether associations with the photometry signal are significant at each timepoint during the behavior. These FLMM output plots display the regression coefficient estimates for each covariate at each timepoint in the trial (solid lines). They also show estimated pointwise (dark-shaded area) and joint (light-shaded area) 95% confidence intervals (CI) for the coefficient estimates. The joint CI allow for the interpretation of each covariate's effect on the photometry signals across multiple time intervals in the trial. Timepoints where the pointwise CI

do not include zero indicate pointwise statistical significance, while timepoints where the joint CI do not include zero indicate joint statistical significance. For the trial order effects we used the FLMM association with continuous variables (https://rpubs.com/gloewinger/1159129). The random intercept model: $\mathbb{E}[Y_{i,j}(s)| X_{i,j}, \gamma_i(s)] = \beta_0(s) + X_{i,j}\, \beta_1(s) + \gamma_{0,i}(s)$ was chosen based on best fit determined by their AIC (Akaike Information Criterion) and BIC (Bayesian Information Criterion) values.

Concurrent FLMM model – We applied a concurrent FLMM model to analyze trials of different lengths and estimate how factors that vary within a trial (e.g., state) influence the photometric signals of PVT^{D2+} neurons. This was necessary as animals took different amounts of time to travel between trigger and reward zones and thus each "trial" could differ in length. Specifically, we included an "approach" variable (a binary indicator of whether an animal was approaching the reward zone at each trial timepoint) in the model, in addition to its interaction with the trial outcome type. For animal *i* on trial *j,* denote:

- $X_{1,I,j}$: the trial outcome, where $X_{1,I,j}$ = 1 for 'strawberry milkshake' (SMS) trials and $X_{1,I,j}$ = 0 for 'other outcome' trials.

- $X_{2,I,j}(s)$: approach, where $X_{2,I,j}(s)$ = 1 when mouse *i* is approaching the reward zone on trial *j* at trial timepoint *s* and $X_{2,I,j}$(s)= 0 for trial timepoints after the reward has been delivered.

- $Y_{i,j}(s)$ is the photometry response of mouse *i* on trial *j* at trial timepoint *s*.

$\beta(s)$ *is* the vector of coefficients at timepoint *s* and $\epsilon_{i,j}(s)$ is Gaussian noise for mouse *i* on trial *j* at trial timepoint *s*.

We used the formula syntax: photometry ~ outcome * approach + (outcome |ID). The model formula was:

$$Y_{i,j}(s) = \beta_0(s) + \gamma_{0,i}(s) + X_{1,i,j}\,[\beta_1(s) + \gamma_1(s)] + X_{2,i,j}(s)\,\beta_2(s) + \beta_3(s)\,X_{1,i,j}\,X_{2,i,j}(s) + \epsilon_{,i,j}(s),$$

where (s) indicates that a variable is functional (i.e., varies across trial timepoints). $X_{1,I,j}$ does not vary with respect to *s*, as it denotes a trial condition.

The coefficients are interpreted:

• β_0(s): The mean signal when a mouse has received (i.e., after reward delivery) an "other" outcome (e.g. a non-caloric reward) at trial timepoint *s*.

• β_1(s): The mean difference in signal between hungry strawberry milk shake reward (H-SMS) and the other outcome (e.g. a non-caloric reward) during reward approach (i.e., before non-caloric reward delivery) at trial timepoint *s*.

• β_2(s): The mean difference between approach and outcome delivery for other outcome trials at trial timepoint *s*.

• β_3(s): This interaction term is interpreted as a difference in differences. Denoting *A*(s) as the mean signal difference between approach and reward in H-SMS (at trial timepoint *s*) trials, and *B*(s) as the mean signal difference (at trial timepoint *s*) between approach and reward in the outcome of comparison (e.g. a non-caloric reward), $\beta_3(s) = A - B$. Thus, $\beta_3(s) = 0$ when the magnitudes of the approach vs. reward zone mean signal difference are equal (at timepoint s) on H-SMS and "other" outcome (e.g. a non-caloric reward) trials. Conversely, $\beta_3(s) \neq 0$ when approaching & H-SMS are together associated with an additional effect. Thus, β_3(s) captures the degree to which the trial outcome type (e.g. H-SMS vs. non-caloric rewards) modulates the change in signal that occurs when an animal receives the reward (compared to approaching the reward zone).

Altogether, this concurrent FLMM model enables a detailed understanding of how context (state and outcome) and behavioral phase (approach vs. outcome delivery) dynamically influence neuronal activity, shedding light on the differences in anticipatory signaling during motivated behavior.

Linear Interpolation - Linear interpolation was used to estimate unknown values that fall within the range of known data points using the following mathematical formula:

$$y = y1 + (x2 - x1)(y2 - y1)(x - x1)$$

In this study, linear interpolation was employed to standardize the length of neuronal recording data across trials of varying durations. This method estimates intermediate values between known data points by assuming a linear relationship. Specifically, here, the recording of each trial was resampled to the same number of data points using linear interpolation, preserving the overall temporal structure while mitigating the effects of varying trial durations. This strategy allowed for consistent alignment and aggregation of neuronal activity patterns across trials. Linear interpolation was solely used to generate averaged traces for graphical purposes showing photometry signals during approach (Fig. 4). These approach signals were analyzed by calculating the AUC of the signal during approach timepoints: for trial *j,* we summed the signal values during approach timepoints and divided that sum by the number of approach timepoints). We then conducted standard hypothesis tests on these AUCs.

Histology

To verify GCaMP6s, hM4Di and TdTomato expression and optical fiber placements, mice were injected with euthanasia solution and subsequently sacrificed via transcardial perfusion, first with PBS and then with paraformaldehyde (PFA; 4% in PBS). Brains were then post-fixed in 4% PFA at 4 °C overnight and cryoprotected using a 30% PBS-buffered sucrose solution for ~24–36 h.

235 Coronal brain sections (50 μm) were generated using a freezing microtome. Images were taken
236 using a Nikon microscope running NIS Elements AR 5.42.03 64-bit (Nikon).

237 **Statistics and data presentation**

238 All data were analyzed using GraphPad Prism (Domatics) and, custom-made Python scripts
239 (Anaconda Navigator). FLMM analyzes were performed using R scripts (R Studio). For the FLMM
240 Trial Order Effects, the associations with continuous variables and random intercept model were
241 used[39-41]. Two-tailed paired and unpaired t-tests (parametric; test statistic: t), repeated measures
242 ANOVAs, and two-way ANOVAs (parametric; test statistic: F). ANOVA was followed by a post-hoc
243 Tukey's, Dunnett's, and Šídák's multiple comparisons test were used when appropriate and if the
244 corresponding omnibus test detected a significant difference. All data are presented as mean ±
245 s.e.m.
246

247 **RESULTS**

248 **PVT^{D2+} neurons sense and track hunger states.**

249 We first examined how physiological states impacted PVT^{D2+} neuronal activity while mice
250 performed a foraging task that assesses motivation. For this, we trained hungry mice to perform
251 a linear foraging task while investigating the *in vivo* dynamics of PVT^{D2+} neurons (Supp Fig. 1A,B).
252 In this task, mice were placed in a linear maze (Supp Fig. 1C) equipped with a reward delivery
253 port and a bright cue LED light at the end wall of the maze (reward zone). The other far end of
254 the maze was set as the "trigger zone". Mice had to learn by trial and error to perform trials
255 requiring them to go and remain in the trigger zone for 2 sec to initiate a rewarded trial, which was
256 signaled by a cue light above the reward port. Once the cue light signaled reward availability, mice
257 could approach the reward zone to obtain a reward (strawberry milkshake, SMS). We found that
258 when mice approached the reward zone, PVT^{D2+} neuronal activity significantly increased (Supp
259 Fig. 1D,E). In accordance with their previous suggested role in sensing interoceptive stimuli, such

260 as hunger, we found that the hunger states modulated PVT^{D2+} neuronal activity. To show this, we
261 first sorted trials performed by trial order, labeling the earliest trials of the session as 'Trial Group
262 - G1' and the latest trials as 'G5'[39] (Supp Fig. 1F). We implemented this strategy to model the
263 assumption that well-trained food-restricted mice are hungrier at the beginning of each 60 min
264 test session than at the end (when they have eaten several rewards). Importantly, here, the
265 average latency to approach did not differ across the trial groups throughout test sessions (Supp
266 Fig. 1G). When comparing between early (G1) and late (G5) trials, the mean PVT^{D2+} neuronal
267 responses were significantly higher in the early trials (Supp Fig. 1H,I), suggesting that stronger
268 hunger levels lead to higher PVT^{D2+} neuronal activity. We also found a strong negative correlation
269 between the area under the curve (AUC) during approach and trial order (Supp Fig. 1J), such that
270 higher PVT^{D2+} neuronal activity was associated with early trials and diminished activity with later
271 trials. The association between trial order and decreases in signal of PVT^{D2+} neurons was
272 confirmed using a functional linear mixed modeling (FLMM) statistical framework[39-41] (Supp Fig.
273 1K). Notably, no correlation was found between approach AUC and latency to approach (Supp
274 Fig. 1L).

275 To further probe the ability of PVT^{D2+} neurons to sense and track hunger levels, we
276 recorded the responses of these neurons during two separate additional test sessions in which:
277 1) Sated mice received a calorie rich SMS reward (Sated- SMS; S-SMS), and 2) hungry mice
278 received a sweet non-caloric reward (Hungry- Non-Cal). Importantly, we used a within-animal
279 comparison strategy to circumvent potential confounds due to differences un viral expression or
280 fiber placement. For these test sessions, we hypothesized that sated mice would display an
281 overall decrease in PVT^{D2+} neuronal activity levels across all trials in the session. Moreover, we
282 also hypothesized that if PVT^{D2+} neurons tracked the hunger levels of the mice when receiving a
283 non-caloric reward (H-NCal), this would result in hungry mice remaining hungry, and thus, PVT^{D2+}
284 neuronal activity would not be modulated across the entire test session. Indeed, we found that
285 when mice were tested in a sated state, a significant decrease in the overall responses of PVT^{D2+}

286 neurons during the reward approach was observed, relative to testing while hungry (Fig. 1A).
287 Comparing trials performed across trial groups in the sated sessions showed significantly higher
288 latencies to approach (Fig. 1B) and steeper decreases in PVT^{D2+} neuronal activity (Fig. 1C-E).
289 PVT^{D2+} neuronal activity during sated states was also negatively associated with trial order (Fig.
290 1F,G), such that lower signals were associated with later trials, but not with latency to approach
291 (Fig. 1H). Conversely, when mice were tested hungry and given a sweet non-caloric reward,
292 PVT^{D2+} neuronal activity significantly increased during the reward approach (Fig. 1I). However,
293 comparing early (G1) and late (G5) group trials in the H-NCal sessions resulted in similar latencies
294 (Fig. 1J), and approach AUCs across group trials (Fig. 1K-M) and the approach AUC was no
295 longer significantly correlated with trial order (Fig. 1N,O) or latency (Fig. 1P). Importantly, mice
296 completed similar number of trials on the caloric (H-SMS), non-caloric (H-NCal), and sated (S-
297 SMS) sessions (Fig. 1Q), suggesting that the decreases in PVT^{D2+} neuronal photometric
298 responses are not solely due to an overall reduction in motivation. Interestingly, in a new cohort
299 of mice tested first while hungry using a caloric reward (H-SMS sessions) and a non-caloric
300 reward (H-NCal sessions), followed by a sated non-caloric reward (S-NCal sessions), we found
301 no differences in the magnitude of the PVT^{D2+} neuronal photometric responses between these
302 three distinct sessions (Fig. 1R-U). These findings show that even when mice are sated, a non-
303 caloric reward still resulted in robust increases in PVT^{D2+} neuronal activity during reward
304 approach. Altogether, these results strongly suggest that PVT^{D2+} neurons can track the internal
305 state of the animal. Additionally, these also suggest that one way they track hunger levels is by
306 sensing the caloric intake.
307

308 **PVT^{D2+} neuronal activity is influenced by the interoceptive value of the outcome.**

309 Our findings showed that a non-caloric reward elicited the same response magnitude
310 regardless of state, indicating PVT^{D2+} neurons might signal the potential interoceptive value of the
311 reward. Indeed, interoceptive value refers to the subjective value assigned to the internal

312 physiological state or bodily sensations used to influence decision-making and behavior
313 signals[2,4,9]. To explore this, we tested whether the interoceptive value of the outcome affected
314 PVT^{D2+} neuronal activity. We compared the responses of PVT^{D2+} neurons during separate
315 sessions where we varied the relative and the interoceptive values of the outcomes. First, we
316 examined the responses of PVT^{D2+} neurons when hungry mice received SMS reward which has
317 a 'higher relative value', 10% sucrose solution (Suc) which has a 'medium relative value', and
318 plain water (H_2O) which has a 'low relative value'. We hypothesized that if PVT^{D2+} neurons were
319 sensitive to the relative value of the reward, switching from SMS to a lower value outcome would
320 decrease the photometric signal during reward approach. However, we found that the response
321 magnitudes during reward approach were similar between H-SMS and H-Suc (Fig. 2A). Trials
322 within the H-Suc sessions also showed state-dependent effects (Fig. 2B-G), though less
323 pronounced than with the calorie-dense SMS reward. Additionally, there was a negative
324 association between PVT^{D2+} neuronal signal and trial order in the H-Suc sessions (Fig. 2F,G).
325 When comparing reward approach during sessions where hungry mice received water (H- H_2O),
326 we observed a significant decrease in PVT^{D2+} neuronal responses (Fig. 2A). This decrease
327 occurred quickly upon encountering the new outcome with no significant differences in signal
328 magnitude between early (G1) and late (G5) trial groups (Fig. 2H-J). In addition, there was no
329 longer an association between signal magnitude and trial order during the approach (Fig. 2K,L),
330 but the FLMM analysis revealed a negative association after reward zone entry (Fig. 2L). These
331 decreases were again likely not due to changes in motivation, as mice performed an equivalent
332 number of trials during water outcome sessions (Fig. 2M). These findings suggest that PVT^{D2+}
333 neurons are activated by behaviors leading to physiologically relevant outcomes, likely encoding
334 interoceptively-valuable stimuli rather than relative value. Indeed, in a 4-bottle choice test, mice
335 strongly preferred the calorie-rich SMS when given the choice between SMS, 10% sucrose, a
336 non-caloric reward, and water (Fig. 2N).

337 To further demonstrate that PVT^{D2+} neurons encode physiologically relevant outcomes, we
338 compared the mean photometric response magnitude of PVT^{D2+} neurons between the following:
339 1) sessions where mice were first tested in the task during hunger and were given the SMS reward
340 (H-SMS), 2) sessions where mice were tested in the task hungry and given the water outcome
341 (H-H_2O), and lastly, 3) test sessions, where mice were given food *ad libitum* and water was
342 restricted and water was given as a reward (T-H_2O). We found that when mice are water restricted
343 and given water as a reward during our task, we again observed the robust increases in the
344 photometric responses of PVT^{D2+} neurons during approach. In addition, the magnitude of the
345 responses was similar to those where mice were tested hungry and given the SMS reward (Fig.
346 2O). Importantly, we again observed state-dependent effects, with higher activity during early trials
347 as compared to late trials (Fig. 2P,Q), and a negative association between signal magnitude and
348 trial order (Fig. 2R,S). Overall, these data strongly suggest that PVT^{D2+} neurons are encoding the
349 behaviors that lead to physiologically relevant outcomes.
350

351 **PVT^{D2+} neuronal activity is state and outcome-dependent.**

352 Our findings showed that motivated behavior engages PVT^{D2+} neurons only when the
353 outcome is physiologically relevant. In other words, PVT^{D2+} neurons are engaged when mice are
354 hungry and are given a food reward or when mice are thirsty and are given a water reward.
355 However, we previously showed that PVT^{D2+} neurons are still active when mice are performing
356 the foraging task and no reward is given[39]. Based on these findings, we hypothesized that PVT^{D2+}
357 neuronal activity remained high during reward omission, because mice were still expecting the
358 reward. To test whether PVT^{D2+} neurons are activated by reward expectation, we performed
359 extended training in our task, for which mice were trained for 8 weeks prior to the omission test
360 (H-SMS). This ensured hungry mice would keep higher response rates despite the reward
361 omission (H-OM), which allowed us to test mice in two consecutive omission sessions to better
362 test the effects of reward expectation in PVT^{D2+} neuronal activity. We also included an additional

363 test session where mice were sated, and the reward was omitted (S-OM). We found that even
364 after extended training, reward approach still resulted in robust PVT^{D2+} neurons photometric
365 responses (H-SMS; Fig. 3A). Next, we found that complete reward omission (H-OM) significantly
366 decreased the overall responses of PVT^{D2+} neurons during reward approach relative to H-SMS
367 sessions (Fig. 3A) and significantly increased the latency to approach (Fig. 3B). In addition, as
368 shown previously, we no longer observed state-dependent modulation of PVT^{D2+} neurons when
369 comparing early (G1) vs late (G5) trial groups (Fig. 3C-E) and we no longer found a significant
370 correlation between approach AUC and trial order (Fig. 3F). Surprisingly, the FLMM analysis
371 uncovered a positive association between trial order and the magnitude of the photometric signal
372 of PVT^{D2+} neurons, such that more trials performed led to higher PVT^{D2+} neuronal responses (Fig.
373 3G). During the sated omission session (S-OM), there was no longer any significant modulation
374 of the responses of PVT^{D2+} neurons by the reward approach (Fig. 3A,H-L). Interestingly, mice in
375 the H-OM session performed significantly more trials than in the H-SMS sessions (Fig. 3M).
376 Altogether, these suggest that decreases in signals were likely not solely due to loss of motivation.
377 To further test the influence of outcome expectation on PVT^{D2+} neuronal activity, we
378 analyzed the photometric responses of PVT^{D2+} neurons during 'premature' trials performed by
379 hungry mice. As mentioned before, in the foraging task, mice had to wait for 2 seconds in the
380 trigger zone to get the cue signaling reward availability. However, we found that in some trials,
381 mice would not properly wait in the trigger zone before deciding to approach, and as a result, the
382 cue signaling the availability was not present during the approach to the reward zone. We
383 categorized those trials as 'premature approaches'. We found that when mice performed
384 premature approaches, there was no significant change in mean PVT^{D2+} neuronal activity during
385 the approach to the reward zone (Fig. 3N). Importantly, the latencies to approach between the
386 "correct" rewarded approaches and unrewarded premature approaches were equal in both trial
387 types (Fig. 3O). Interestingly, we again observed state-dependent effects, with higher activity
388 during early trials 'G1' as compared to late trials 'G5' in the premature trials (Fig. 3P,Q). These

389 findings suggest that PVT^{D2+} neuronal activity is modulated within a session depending on
390 outcome expectation.

391 Next, we sought to test the hypothesis that PVT^{D2+} neurons are responding to two
392 dissociable events: 1) The outcome expectation during approach, and 2) The outcome itself.
393 However, since our task is fully self-paced, trials performed have different latencies, and thus
394 averaging trials by 'trial group' does not allow us to fully dissociate between the reward
395 expectation during approach and reward delivery. As such, to determine whether we could fully
396 dissociate the responses of PVT^{D2+} neurons between 'approach only' and 'reward only', we
397 performed two different, yet complementary, analyses. For the first analysis, we limited each trial
398 to approach only or reward delivery-only and calculated the AUC for each approach trial in each
399 outcome group. This strategy allowed us to analyze approach and reward delivery separately.
400 During approach, we found that, in most test sessions, correct trials led to higher PVT^{D2+} neuronal
401 responses as compared to premature trials (Fig. 4A-F, M). The magnitude of the responses for
402 the approach was modulated by the expected outcomes such that test sessions with higher
403 relative value outcomes (H-SMS) had stronger responses as compared to less valuable outcomes
404 (Fig. 4A-F). Surprisingly, during H-OM sessions, we found no differences between the responses
405 of PVT^{D2+} neurons for correct and premature trials (Fig. 4F,M). These effects were likely due to
406 the ambiguity created by not receiving an outcome in either trial type for the H-OM test sessions.
407 In contrast, receiving an outcome, even if not rewarding (i.e., H_2O), made it clear that the task
408 contingencies had not changed, only the outcome. As a result, the expectation is lower than when
409 receiving no outcome. Next, we isolated and compared the responses of PVT^{D2+} neurons to
410 reward delivery and feeding bouts. We found that photometric responses of PVT^{D2+} neurons to
411 the reward delivery also depended upon the outcome and state of the mice (Fig. 4G-L). We again
412 found significant state-dependent changes in the signal of PVT^{D2+} neurons within each session
413 that provided a caloric reward (Fig. 4G,H,J,N). These state-dependent responses were not

414 observed in the sessions that did not provide a caloric reward: H-NCal (Fig. 4I,N), the H- H_2O
415 (Fig. 4E,N), and H-OM sessions (Fig. 4F,N).

416 For the second analysis, we used a concurrent FLMM, which allows for between session
417 comparisons while accounting for differing trial lengths. We did this by inclusion of a binary a
418 functional covariate (i.e., a covariate whose values could change across trial timepoints) that
419 indicated timepoints when the animal was approaching a reward (as opposed to timepoints after
420 reward delivery). This concurrent FLMM model also enabled us to investigate how context (state
421 and outcome) and behavioral phase (approach vs. outcome delivery) dynamically influence the
422 photometric responses of PVT^{D2+} neurons. Our new concurrent FLMM analysis confirmed our
423 findings and uncovered additional differences missed by our averaging approach (Supp. Fig. 2).
424 Here, we found that for substantial portions of the time animals were in the reward delivery zone,
425 the mean photometry signal in the H-SMS conditions was significantly higher than in the S-SMS
426 (Supp. Fig. 2A $\beta_1(s)$), H-H_2O (Supp. Fig. 2D $\beta_1(s)$) and the H-OM conditions (Supp. Fig. 2E $\beta_1(s)$).
427 In contrast, when comparing the H-SMS and the H-NCal conditions, we found the mean
428 photometry signal was significantly higher in the H-NCal than the H-SMS during the late stages
429 of the reward delivery (Supp. Fig. 2B $\beta_1(s)$). This confirms that PVT^{D2+}neurons respond similarly
430 to caloric and non-caloric rewards, yet non-caloric rewards do not induce state-dependent
431 decreases in the later stages of the feeding bouts. Additionally, no differences in the mean signal
432 magnitude were found when comparing the H-SMS and H-Suc conditions during reward delivery
433 (Supp. Fig. 2C $\beta_1(s)$), again suggesting that these neurons do not encode the relative value of the
434 outcome. Using the concurrent FLMM model, we also found that in all conditions, the mean signal
435 was lower during approach than reward delivery (Supp. Fig. 2A-E $\beta_2(s)$). *)*). Lastly, this FLMM
436 model enabled us to evaluate the interaction effects between behavioral states (e.g., approaching
437 vs. receiving), internal states (e.g., hungry vs. sated), and outcome types (e.g., SMS vs. NCal),
438 and how these factors collectively influence the neural response of PVT^{D2+} neurons (Supp. Fig.
439 2A-F $\beta_3(s)$). Specifically, we observed that the interaction for the H-SMS vs. S-SMS comparison

440 is negative, indicating that the mean differences in photometric responses between these two
441 outcome types are larger during the outcome delivery than during outcome approach. The results
442 were similar for the interaction in the H-SMS vs. H-H_2O comparisons (Supp. Fig. 2D $\beta_3(s)$). For
443 the H-SMS vs. NCal comparison, we found that the interaction is first negative and then is positive,
444 showing that the differences in mean neural activity between approach and reward delivery
445 timepoints is lower in H-NCal (than H-SMS) during early portions of the trial. Then, during later
446 portions of the trial, the difference in mean signals between approach and reward timepoints is
447 higher in the H-SMS condition (Supp. Fig. 2B $\beta_3(s)$). Again, we found no differences between H-
448 SMS and H-Suc (Supp. Fig. 2C $\beta_3(s)$). Finally, for the H-SMS vs. H-OM comparison, we found
449 that the interaction is first positive and then is negative, showing that the differences in neural
450 activity between approach and reward timepoints are higher in H-OM than in H-SMS during early
451 portions of the trial. Then during later portions of the trial, the difference in mean signals between
452 approach and reward timepoints is higher in the H-OM condition (Supp. Fig. 2E $\beta_3(s)$). This
453 suggests that for extensively trained mice accustomed to expecting a reward, receiving no
454 outcome might lead to initial ambiguity regarding reward expectation, particularly early in the trials.
455 This contrasts with receiving a bad outcome (as in H- H_2O conditions). Collectively, the findings
456 from the concurrent FLMM models suggest that most of the changes in photometric signal from
457 PVT^{D2+} neurons are due to differences in the signal from the behavioral phase, outcome expected,
458 and state of the animal.
459

460 **PVT^{D2+} neuronal activity during return is modulated by state, outcome, and outcome**
461 **expectation.**

462 Next, we sought to test the *in vivo* dynamics of these PVT^{D2+} neurons during the return
463 from the reward zone to the trigger zone. We reasoned that by examining the *in vivo* dynamics
464 during this time, where mice are engaging in the same motivated behavior (running) but not
465 expecting a reward, it would allow us to further dissociate the PVT^{D2+} neuronal responses between

466 expectation of the outcome and the outcome delivery. Interestingly, we found returning from the
467 reward zone to the trigger zone resulted in a robust decrease in the photometric responses of
468 PVT^{D2+} neurons in all outcome sessions (Fig. 5). Moreover, the responses were also robustly
469 modulated depending on the state of the mice (Fig. 5A,B,D,G), the outcome delivered (Fig. 5A-
470 G), and the outcome expectation. Surprisingly, our analysis of trial group by comparing early 'G1'
471 vs. late trials 'G5' revealed very robust state-dependent differences in those sessions where
472 caloric outcomes were provided (Fig. 5A,B,D), such that stronger decreases in the signal of
473 PVT^{D2+} neurons were observed in early trials as compared to late trials. These effects again were
474 absent in those sessions where non-caloric outcomes were provided (H-NCal, H- H_2O, and H-
475 OM sessions; Fig. 5C,E,F). These differences in photometric responses during return between
476 outcome groups (Fig. 5G) and across trial groups were unlikely due to differences in baseline
477 activity prior to return. Indeed, we analyzed the time spent in the reward zone post-reward delivery
478 (Supp. Fig. 3), which showed no significant differences in reward zone durations across all
479 outcome groups (Supp. Fig. 3G). Moreover, mice spent an average of approximately 20 seconds
480 in the reward zone prior to return (Supp. Fig. 3G), and by then, the signal increases resulting from
481 reward delivery (10-second analysis) had returned to baseline in most outcome groups (Fig. 3G-
482 L). Lastly, our analysis comparing time spent in the reward zone post-reward delivery also showed
483 no significant differences in any of the outcome groups (Supp. Fig.3A-F). Altogether, these
484 findings strongly suggest that PVT^{D2+} neuronal activity during return is modulated by state,
485 outcome, and outcome expectation.
486

487 **Motivational states are associated with PVT^{D2+} neuronal responses across different**
488 **conditions.**

489 Our findings showed that PVT^{D2+} neurons mediate interoceptive predictions by integrating
490 information about the animal's state and the expected outcome. Previously, we demonstrated that
491 PVT^{D2+} neuron activity was closely linked to the latency to approach the reward zone in a linear

492 foraging task[39]. Based on these findings, we hypothesized that PVT^{D2+} neuronal activity is
493 associated with latency to approach because latency reflects the motivational strength of the
494 interoceptive prediction. Specifically, lower latencies (fast trials) would be associated with higher
495 predictions and thus higher PVT^{D2+} neuronal responses, while higher latencies (slow trials) would
496 be associated with weaker predictions and thus attenuated PVT^{D2+} neuronal responses. Thus, we
497 reasoned that the link between approach latency and PVT^{D2+} neuronal responses would be
498 modulated by the animal's state, the outcome, and the outcome expectation. To test this, we
499 sorted all trials across different conditions by latency to approach, labeling the fast trials as
500 'Latency Group - L1' and the slow trials as 'L5'[39] (Supp Fig. 4). We then calculated the slope of
501 the line for each latency group under the different conditions. The approach slope has been shown
502 to reflect latency changes in PVT^{D2+} neuronal responses, whereas the area under the curve (AUC)
503 does not[39]. Consistent with previous findings, we found significant correlations between latency
504 to approach and the approach slope across most conditions: H-SMS (Supp. Fig. 4A), S-SMS
505 (Supp. Fig. 4B), H-NCal (Supp. Fig. 4C), H-Suc (Supp. Fig. 4D), and H-OM (Supp. Fig. 4F). As
506 such, fast trials (L1) correlated with higher approach slopes, while slow trials correlated with lower
507 approach slopes. Interestingly, we found this latency mediated modulation was lost in the H- H_2O
508 (Supp. Fig. 4E) and the S-OM conditions (Supp Fig. 4G). These results suggest that associations
509 between PVT^{D2+} neuronal activity and latency to approach reflects the motivational strength of the
510 interoceptive prediction.
511
512 **PVT^{D2+} neurons detect changes in reward magnitude.**
513 Interoception models have posited that brain areas encoding interoceptive predictions
514 have the capability to detect changes in reward magnitude[4-6,9,42]. Since interoceptive predictions
515 help anticipate and regulate bodily conditions, they inherently detect changes in reward
516 magnitude which allows the brain to efficiently allocate effort and attention to optimizing resource
517 acquisition[4,42]. As such, we next tested whether PVT^{D2+} neurons could detect changes in reward

518 magnitude. To investigate this, we first trained hungry mice to perform the linear foraging task to
519 obtain a non-caloric reward (Fig. 6A). We used a non-caloric reward to avoid state-dependent
520 changes that could confound our results. Once we confirmed this during a pre-test (Fig. 6B, E),
521 the mice underwent a 'reward magnitude test session' consisting of three within-session trial
522 blocks, each offering different reward sizes (small: 1µl, medium: 3µl, and large: 6µl; Fig. 6A). We
523 found that PVT^{D2+} photometric responses were modulated by the different reward magnitudes,
524 such that bigger rewards resulted in higher response signaling of these neurons, while smaller
525 reward magnitudes resulted in lower response magnitudes (Fig. 6C). No significant changes in
526 approach latency were found between reward magnitude trial blocks (Fig. 6D). Interestingly,
527 different reward magnitudes did not change the photometric responses during return (Fig. 6F,G).
528 Altogether, these findings strongly suggests that PVT^{D2+} neurons can detect changes in reward
529 magnitude.
530
531 **PVT^{D2+} neuronal responses emerge from learned cue-outcome associations.**
532 Brain areas involved in interoceptive predictions also have the distinct ability to predict
533 internal states based on the current state, expected outcomes, and learned environmental cues[4-
534 6,9]. Thus, we next tested whether PVT^{D2+} neuronal responses also depend on the environmental
535 cues associated with the outcome and state. Indeed, we showed that when mice returned from
536 the reward zone to the trigger zone in the foraging task, the photometric responses of PVT^{D2+}
537 neurons displayed robust decreases that were state and outcome dependent (Fig. 5). Thus, we
538 hypothesized that the differences in PVT^{D2+} neuronal responses between the reward approach
539 and the return to the trigger zone could be due to the learned association between a side of the
540 maze and the outcome associated with it (reward zone = reward vs. trigger zone = no reward). If
541 the increases in PVT^{D2+} neuronal activity during the approach, and decreases during the return,
542 are due to the learned cue-outcome associations, then these would appear gradually as mice
543 learn to associate each side of the maze with their respective outcome. To test this, we assessed

544 the photometric responses of PVT^{D2+} neurons as mice learned to perform our linear foraging task.
545 Here, we first exposed mice to the SMS and ensured mice were consuming it reliably. We found
546 a small modulation of PVT^{D2+} neuronal responses during the reward approach (Fig. 7A) and
547 during the return to the trigger zone (Fig. 7D) throughout the first training session (S1). However,
548 as mice received more training sessions and learned to associate the reward zone with the
549 delivery of the SMS and the return with the lack of reward, the PVT^{D2+} neuronal responses during
550 approach (Fig. 7A) and during return emerged (Fig. 7D) in a training- and session-dependent
551 manner. To identify precisely when responses emerged, we compared the dynamics between the
552 early trial group (G1) versus the late trial group (G5) in training session 1. Surprisingly, no
553 differences were found between them (Fig. 7G,I). We then analyzed training session 2 (Fig. 7H,J)
554 and compared the dynamics between the early (G1) versus late trial group (G5). Again, we found
555 small increases in the overall activity of the PVT^{D2+} neurons that were present even in the early
556 trial group (G1). These increases were slightly bigger in late trials of both sessions (Fig. 7G, H),
557 however these were not statistically significant. Notably, the lack of within-session ('G1' vs. 'G5')
558 statistical differences for S1 and S2 sessions is likely due to responses being occluded by the
559 satiety effects present, particularly in later trials. Nonetheless, these findings show that these
560 neuronal responses emerge slowly despite successful task acquisition, as evidenced by the
561 increases in trials performed during later sessions (Fig. 7C). For the return responses, we found
562 similar dynamics in the emergence of the responses (Fig. 7I,J). However, by session 2, we found
563 significant difference between early and late trials (Fig. 7J), presumably due to the certainty of not
564 receiving a reward after return. Altogether, these findings show that PVT^{D2+} neuronal responses
565 develop as mice learn cue-outcome associations. These findings are also in accordance with the
566 new proposed role of PVT^{D2+} neurons in the signaling of interoceptive predictions. Indeed, it has
567 been suggested that predictive interoceptive responses develop more slowly than exteroceptive
568 predictions[4] because interoceptive signals tend to be subtler and more diffused than exteroceptive
569 signals[4].

570 **Chronic PVT^{D2+} neuronal inhibition impairs performance in the foraging tasks.**

571 Since PVT^{D2+} neurons encode interoceptive predictions and their responses emerge
572 slowly, across several sessions, we then aimed to investigate whether chronic chemogenetic
573 inhibition of PVT^{D2+} neurons would impair performance in our foraging task. To do this, D2-Cre
574 mice were injected with either an AAV-hSyn-DIO-hM4D(Gi)-mCherry virus or a control virus (AAV-
575 CAG-Flex-TdTomato) in the PVT. Once the virus was expressed, hM4Di- PVT^{D2+}mice and control-
576 PVT^{D2+} mice were injected with CNO and trained in the linear foraging task (Fig. 8A,B). Given that
577 PVT^{D2+} neuronal responses were slow to emerge, we repeated our chemogenetic inhibition for
578 three test sessions, followed by three sessions in which the mice were injected with saline prior
579 to testing (Fig. 8B). We found that chemogenetic inhibition of PVT^{D2+} did not result in acute
580 changes in performance for both correct (Fig. 8C) and premature trials (Fig. 8E). We found
581 significant differences in the latencies to perform correct (Fig. 8D) and premature trials (Fig. 8F);
582 but, these were not consistent across the three CNO test sessions. However, we found that when
583 mice were tested for post-inhibition effects, control mice performed a significantly higher number
584 of correct trials compared to hM4Di-PVT^{D2+} mice (Fig. 8C). No changes in the performance of
585 premature trials were observed between controls and hM4Di-PVT^{D2+} mice during post-inhibition
586 testing (Fig. 8E). These data indicate that PVT^{D2+} neurons are not required for task acquisition,
587 but inhibition of these neurons impair the long-term performance of interoceptive-guided
588 motivated behavior.

589

590 **DISCUSSION**

591 In this study, we characterized a specific role for PVT^{D2+} neurons in using interoceptive
592 cues to guide goal-directed behavior. We showed that PVT^{D2+} neurons compute an interoceptive
593 prediction by integrating factors, such as current physiological needs, previous experiences, and
594 environmental cues to guide motivated behavior. Using a linear foraging task that assesses
595 motivated behavior in combination with *in-vivo* fiber photometry of PVT^{D2+} neurons, we found a

596 significant increase in the response of these neurons during reward approach and reward delivery.
597 Furthermore, these increases are directly related to the current state of the animal, but also
598 depend on the outcome expectation. We only observed increases in PVT^{D2+} neuron activity during
599 motivated behavior of hungry animals expecting a food reward, but not during motivated behavior
600 of hungry animals expecting a water outcome, or during the return to the trigger zone. In addition,
601 when mice were thirsty and a water outcome was provided, these neurons again showed these
602 increases during reward approach.
603
604 **Sensing of current physiological states by PVT neurons**
605 Previous anatomical and functional studies have already established the PVT as a critical
606 hub for sensing and responding to changes in homeostasis[15-17]. These studies highlighted the
607 role of PVT neurons as key detectors of homeostatic imbalances, including changes in energy
608 levels[18,29,43-48], hydration[13,14,49], stress[26-28,50], pain[23-25], thermoregulation[21,22], itch[51,52], social
609 behavior[53-55], and arousal states[56-58]. Anatomically, PVT neurons are richly connected to brain
610 regions that monitor these homeostatic signals, such as the hypothalamus, which relays
611 information about hunger, thirst, and stress through hormonal and neuropeptide signals, including
612 orexin[18,59,60], neuropeptide Y[19], and others[61]. The PVT also shares rich connections with brainstem
613 areas, such as rostral ventrolateral medulla[29] and the nucleus of the solitary tract[46], which receive
614 information about the state of the body through somatic afferents and chemosensory receptors[11].
615 Furthermore, PVT neurons express some of these chemosensory receptors, which
616 enables them to directly sense and respond to homeostatic challenges. For example, PVT
617 neurons express the Glut2 glucose transporter and are capable of directly detecting glucose
618 levels[62]. Electrophysiological recordings show that glucose directly modulates the firing activity of
619 PVT neurons, with some neurons exhibiting increased excitability in response to low glucose
620 levels[62]. PVT neurons also sense changes in extracellular glucose concentrations via expression
621 of enzymes like glucokinase[47]. Moreover, changes in hydration status, such as dehydration,

activate PVT neurons, which in turn promote thirst-related behaviors[13,14]. Beyond basic survival needs, the PVT contributes to maintaining arousal and circadian rhythms, responding to dynamic changes in sleep-wake states and coordinating transitions between them[37,56,63]. Similarly, the PVT regulates stress responses via inputs from the hypothalamus and brainstem and projections to the amygdala and prefrontal cortex, influencing both emotional and physiological adaptations[26,27,33-35,64]. Experimental manipulation of PVT activity using optogenetics and chemogenetics further underscores its role in homeostasis. For instance, activating or inhibiting specific PVT subpopulations can alter feeding[18,31], drinking[13,14], stress reactivity[26,33,35], and arousal levels[37,57]. Collectively, our findings are consistent with previous research showing that the magnitude of the activity of PVT neurons encodes the salience of current internal states, such as the degree of hunger or the level of stress. We also expand on this knowledge by showing that PVT^{D2+} neurons are likely involved in these state-dependent processes.

Notably, in our study, we also found that a non-caloric reward showed increased PVT^{D2+} neuronal responses during reward approach and reward delivery for both hunger and sated states. This was somewhat surprising given that a non-caloric reward presumably does not relay information about nutritional value or physiological significance. However, when these non-caloric rewards were provided, we no longer observed within-session state-dependent modulation. Other studies also find differences in neurocircuit involvement following non-caloric sweetener consumption. The intake of the non-caloric sweetener, sucralose, fails to deactivate hypothalamic areas compared to the ingestion of glucose and fructose[65]. Additionally, sucralose consumption reduces activity of midbrain areas related to reward, including the lateral hypothalamus (LHA), ventral tegmental area (VTA), and nucleus accumbens (NAc) as compared to caloric options[66]. However, despite their wide use, relatively little is known about the effects of non-caloric sweeteners in the brain. Indeed, one of the suggested potential risks of non-caloric food intake is the decoupling of sweet taste from the satiety effects needed for maintaining the finely tuned regulation of energy homeostasis[67]. Future research should investigate the underlying

648 mechanisms of how sweet tastants activate PVT^{D2+} neurons and the observed decoupling of
649 reward and satiety we observed.
650
651 **Modulation of PVT^{D2+} neurons by environmental cues and context**
652 Previous studies established that PVT neurons are particularly sensitive to external
653 signals that predict outcomes critical for survival, such as food, safety, or danger[18,19,27,32,33,35,46,58].
654 When an environmental cue is associated with a physiologically relevant outcome, PVT neurons
655 become activated by the predictive cues[18,33]. This activation is proposed to facilitate the integration
656 of relevant sensory information enabling the prediction of future internal physiological states to
657 drive adaptive responses accordingly. For instance, in a hunger state, the PVT exhibits
658 heightened activity in response to food-related cues[18]. This heightened response to
659 physiologically relevant cues has been documented in other states like thirst[13,14], fear[26,33,35],
660 safety[27], and social[54] behaviors. These responses engage with downstream brain regions like the
661 NAc[18,26,29,39], amygdala[24,33,35] and prefrontal cortex[27,30,33,34] to prioritize behaviors that will
662 reestablish homeostasis[13,15,29,68]. We confirmed and expanded this previous knowledge by
663 showing that cues and context modulated the responses of PVT^{D2+} neurons, as shown by the
664 differential responses to the reward zone approach vs. trigger zone return (Fig. 1 and Fig. 6) and
665 of correct vs. premature trials (Fig. 4N). These context and cue-driven activations reflect the ability
666 of PVT^{D2+} neurons to dynamically adjust their activity based on the motivational significance of the
667 stimulus, ensuring that resources are directed toward the most urgent physiological needs.
668 Additionally, a major finding of this study is the slow emergence of these cue-induced responses,
669 which are in contrast to the fast emergence of cue-induced responses in other brain regions[33,34,69].
670 Indeed, the slow emergence of cue related responses in PVT neurons have been previously
671 documented in the literature[33,34] and are in accordance with our new proposed role of PVT^{D2+}
672 neurons in driving interoceptive predictions. This is consistent with modern interoceptive models,
673 which posit that predictive interoceptive responses to environmental cues tend to emerge at a

674 much slower pace than exteroceptive predictions[4,5,9]. This slow emergence has been attributed
675 to interoception signals being more subtle and diffused than exteroceptive ones[4,5]. Importantly,
676 dysregulation of cue-driven activation has been implicated in conditions like substance use
677 disorder, where maladaptive cue-responses lead to compulsive behaviors. This highlights the
678 critical balance the PVT^{D2+} neurons might maintain in the processing and prioritizing of
679 environmental stimuli.
680

681 **Modulation of PVT^{D2+} neurons by learned experiences and their role in interoceptive**
682 **predictions**

683 Models of interoception also posit that beyond sensing of current internal signals from the
684 body, the brain also makes predictions of future internal states[3-6,9]. Indeed, these same models
685 postulate that predictive coding of internal states are not represented in a single brain area but in
686 the connectivity of various hierarchical populations of neurons. This hierarchy enables
687 representation at various levels of abstraction, with higher levels integrating information across
688 multiple sensory domains to create more abstract predictions, while lower levels integrate more
689 exact sensory inputs[9]. Previous studies in humans and rodents show that one key higher-level
690 area involved in these predictions is the insula cortex[1,49,70]. Importantly, the PVT shares strong
691 anatomical connections with the insula cortex neurons that participate in the predictive coding of
692 future internal states[49,71]. Here, we also expand on this knowledge to show that PVT^{D2+} neurons
693 are part of the hierarchy of populations making predictions of internal states. We now show that
694 beyond their role in detecting current internal states, PVT^{D2+} neurons also dynamically adjust their
695 activity to reflect both the internal state of the organism and the expected value of the outcome.
696 This was most obviously demonstrated by the increased PVT^{D2+} neuronal activity observed when
697 mice were approaching the reward zone. Conversely, the same motivated behavior, 'running'
698 towards the trigger zone, resulted in profound decreases in the responses of these neurons.
699 Importantly, and consistent with their ability to make interoceptive predictions, the responses

700 during return were also modulated by the state of the animal and the expectation of the outcome.
701 Even though mice were not directly rewarded for returning to the trigger zone, we still observed
702 state-dependent effects in sessions where caloric outcomes were provided, but not in those
703 sessions where non-caloric outcomes were provided. In addition, analyzing premature
704 approaches allowed us to assess the responses of PVT^{D2+} neurons while animals ran with the
705 same vigor and in the same context (toward the reward zone) but without a cue light signaling the
706 reward. During these premature approaches, we no longer observed increases in the activity of
707 PVT^{D2+} neurons during approach. Moreover, these differences between correct and premature
708 responses were not observed when the outcome was no longer relevant (Hungry- H_2O sessions
709 and Hungry- OM sessions). These findings strongly suggest that when the outcome is not
710 relevant, PVT^{D2+} neurons adjust their activity to update future interoceptive predictions.
711

712 **Interoception deficits as a major underlying mechanism for prominent psychiatric**
713 **conditions**

714 Interoception is one of the core drivers of motivation and emotion[2-4,6,8]. However, when
715 interoceptive systems become dysregulated, it can lead to motivational and emotional deficits
716 seen in many prominent psychiatric conditions, including chronic stress, major depressive
717 disorder (MDD), autism spectrum disorders (ASDs), and others[2,3,6,8]. Both human and rodent
718 studies show that the paraventricular thalamus (PVT) contributes to these disorders in different
719 ways. For example, chronic stress manifests physiologically with increases in cortisol levels
720 and/or impaired hypothalamus-pituitary-adrenal (HPA) axis activation[72,73]. PVT activity is altered
721 after chronic stress[26,74] , and lesions or inactivation of the PVT impair animals' ability to adapt to
722 novel stressors[28]. MDD, characterized by low mood and low motivation, is highly linked to
723 autonomic dysfunction and inflammation[75]. Studies in animals show that inflammation results in
724 PVT dysfunction and motivational impairments[76-79], indicating that dysregulation of PVT neuorns
725 could be a key driver of low motivation in MDD. Additionally, anxiety disorders, eating disorders,

726 substance use disorders, and pain disorders are other well-known conditions resulting from
727 dysregulation of interoceptive processes[2,3,6,8]. The PVT has been implicated in these conditions
728 in both humans and rodents[80].
729
730 **Limitations**
731 The present study used fiber photometry to investigate the activity of PVT^{D2+} neurons and
732 their role in interoceptive signaling and predictions. It is possible that the observed PVT neuronal
733 activity includes averaged responses from other PVT subpopulations beyond PVT^{D2+} neurons.
734 However, other neuronal types, such as PVT neurons that do not express the D2 receptor, have
735 not shown state-dependent changes[39]. Additionally, a recent study examining the activity of
736 anterior PVT neurons (where most D2- neurons are expressed) found that these neurons were
737 not modulated by state or satiety[81]. Future studies, however, should use single-cell calcium
738 imaging of PVT neurons to fully characterize the activity of PVT^{D2+} and PVT^{D2-} neurons during
739 interoceptive prediction. This approach will help understand the impact of factors such as
740 physiological states, environmental cues, and previous experiences on these neurons and the
741 encoding of interoceptive predictions.
742 In conclusion, pinpointing the functional role of PVT neurons and their contribution to
743 motivated behavior has been challenging. This difficulty arises from the recently discovered
744 heterogeneity in PVT neurons[37-39,82] and their opposing functional responses[39]. Additionally, the
745 PVT has been implicated in various conditions and roles, adding to the complexity. The findings
746 presented here illuminate the role of PVT^{D2+} neurons in mediating interoceptive predictions,
747 proposing a more unified role that contextualizes previous findings. Collectively, and as
748 highlighted here, interoception signaling and predictions are central to creating internal states that
749 guide adaptive behavior. Dysregulation of interoceptive processes result in a range of psychiatric
750 and neurological conditions. Thus, a deeper understanding of the neural basis of interoception
751 may offer new insights into potential therapeutics for these debilitating conditions. By elucidating

key areas and neuronal populations involved and how they respond to different factors, this research may help identify new therapeutic targets aimed at restoring healthy interoceptive signaling in individuals.

ACKNOWLEDGEMENTS

We thank Drs. Zachary Knight, Kirstie Cummings, Jamie Peters, Barry Setlow, and Chase Francis for their comments on the manuscript. This work was supported by Department of Neurobiology at the University of Alabama Birmingham, an R00 MH126429 to S.B., a NARSAD Young Investigator Award by the Brain and Behavior Research Foundation to S.B., a T32 by the National Cancer Institute of the National Institutes of Health under award number T32CA047888 to B.M., a NIGMS K12 Institutional Research and Career Development Award to S.N.M. and by the NIMH Intramural Research Program (project ZIC-MH002968, authors A.X., F.P., and G.L.).

AUTHOR CONTRIBUTIONS

B.M., C.L., and S.N.M. performed the behavioral experiments and surgeries. L.A., and J.T. assisted with behavioral experiments and histology. B.M. and S.B. performed all the data analysis. A. X., G.L., and F.P. assisted with the FLMM concurrent model analyses. S.B. designed the study and interpreted the results. S.B. wrote the manuscript. B.M., S.N.M., and G.L., provided extensive edits and comments to the manuscript.

COMPETING INTERESTS

The authors declare no competing interests. This content is solely the responsibility of the authors and does not necessarily represent the views of the NIH.

REFERENCES

1. Chen, W.G., Schloesser, D., Arensdorf, A.M., Simmons, J.M., Cui, C., Valentino, R., Gnadt, J.W., Nielsen, L., Hillaire-Clarke, C.S., Spruance, V., et al. (2021). The Emerging Science of Interoception: Sensing, Integrating, Interpreting, and Regulating Signals within the Self. Trends Neurosci *44*, 3-16. 10.1016/j.tins.2020.10.007.
2. Khalsa, S.S., Adolphs, R., Cameron, O.G., Critchley, H.D., Davenport, P.W., Feinstein, J.S., Feusner, J.D., Garfinkel, S.N., Lane, R.D., Mehling, W.E., et al. (2018). Interoception and Mental Health: A Roadmap. Biol Psychiatry Cogn Neurosci Neuroimaging *3*, 501-513. 10.1016/j.bpsc.2017.12.004.
3. Quadt, L., Critchley, H.D., and Garfinkel, S.N. (2018). The neurobiology of interoception in health and disease. Ann N Y Acad Sci *1428*, 112-128. 10.1111/nyas.13915.
4. Feldman, M.J., Bliss-Moreau, E., and Lindquist, K.A. (2024). The neurobiology of interoception and affect. Trends Cogn Sci *28*, 643-661. 10.1016/j.tics.2024.01.009.
5. Berntson, G.G., and Khalsa, S.S. (2021). Neural Circuits of Interoception. Trends Neurosci *44*, 17-28. 10.1016/j.tins.2020.09.011.
6. Tsakiris, M., and Critchley, H. (2016). Interoception beyond homeostasis: affect, cognition and mental health. Philos Trans R Soc Lond B Biol Sci *371*. 10.1098/rstb.2016.0002.
7. Adolfi, F., Couto, B., Richter, F., Decety, J., Lopez, J., Sigman, M., Manes, F., and Ibanez, A. (2017). Convergence of interoception, emotion, and social cognition: A twofold fMRI meta-analysis and lesion approach. Cortex *88*, 124-142. 10.1016/j.cortex.2016.12.019.
8. Bonaz, B., Lane, R.D., Oshinsky, M.L., Kenny, P.J., Sinha, R., Mayer, E.A., and Critchley, H.D. (2021). Diseases, Disorders, and Comorbidities of Interoception. Trends Neurosci *44*, 39-51. 10.1016/j.tins.2020.09.009.
9. Petzschner, F.H., Garfinkel, S.N., Paulus, M.P., Koch, C., and Khalsa, S.S. (2021). Computational Models of Interoception and Body Regulation. Trends Neurosci *44*, 63-76. 10.1016/j.tins.2020.09.012.
10. Saper, C.B., Chou, T.C., and Elmquist, J.K. (2002). The need to feed: homeostatic and hedonic control of eating. Neuron *36*, 199-211. 10.1016/s0896-6273(02)00969-8.
11. Zimmerman, C.A., and Knight, Z.A. (2020). Layers of signals that regulate appetite. Curr Opin Neurobiol *64*, 79-88. 10.1016/j.conb.2020.03.007.
12. Grove, J.C.R., and Knight, Z.A. (2024). The neurobiology of thirst and salt appetite. Neuron *112*, 3999-4016. 10.1016/j.neuron.2024.10.028.
13. Leib, D.E., Zimmerman, C.A., Poormoghaddam, A., Huey, E.L., Ahn, J.S., Lin, Y.C., Tan, C.L., Chen, Y., and Knight, Z.A. (2017). The Forebrain Thirst Circuit Drives Drinking through Negative Reinforcement. Neuron *96*, 1272-1281 e1274. 10.1016/j.neuron.2017.11.041.
14. Allen, W.E., DeNardo, L.A., Chen, M.Z., Liu, C.D., Loh, K.M., Fenno, L.E., Ramakrishnan, C., Deisseroth, K., and Luo, L. (2017). Thirst-associated preoptic neurons encode an aversive motivational drive. Science *357*, 1149-1155. 10.1126/science.aan6747.
15. Penzo, M.A., and Gao, C. (2021). The paraventricular nucleus of the thalamus: an integrative node underlying homeostatic behavior. Trends Neurosci *44*, 538-549. 10.1016/j.tins.2021.03.001.
16. McGinty, J.F., and Otis, J.M. (2020). Heterogeneity in the Paraventricular Thalamus: The Traffic Light of Motivated Behaviors. Front Behav Neurosci *14*, 590528. 10.3389/fnbeh.2020.590528.

17. Kirouac, G.J. (2015). Placing the paraventricular nucleus of the thalamus within the brain circuits that control behavior. Neurosci Biobehav Rev *56*, 315-329. 10.1016/j.neubiorev.2015.08.005.
18. Meffre, J., Sicre, M., Diarra, M., Marchessaux, F., Paleressompoulle, D., and Ambroggi, F. (2019). Orexin in the Posterior Paraventricular Thalamus Mediates Hunger-Related Signals in the Nucleus Accumbens Core. Curr Biol *29*, 3298-3306 e3294. 10.1016/j.cub.2019.07.069.
19. Horio, N., and Liberles, S.D. (2021). Hunger enhances food-odour attraction through a neuropeptide Y spotlight. Nature *592*, 262-266. 10.1038/s41586-021-03299-4.
20. Betley, J.N., Cao, Z.F., Ritola, K.D., and Sternson, S.M. (2013). Parallel, redundant circuit organization for homeostatic control of feeding behavior. Cell *155*, 1337-1350. 10.1016/j.cell.2013.11.002.
21. Kanai, M., Kamiizawa, R., Hitora-Imamura, N., and Minami, M. (2022). Exposure to hot and cold environments activates neurons projecting from the paraventricular thalamic nucleus to brain regions related to approach and avoidance behaviors. J Therm Biol *103*, 103157. 10.1016/j.jtherbio.2021.103157.
22. Bhatnagar, S., and Dallman, M.F. (1999). The paraventricular nucleus of the thalamus alters rhythms in core temperature and energy balance in a state-dependent manner. Brain Res *851*, 66-75. 10.1016/s0006-8993(99)02108-3.
23. Mindaye, S.A., Chen, W.H., Lin, S.C., Chen, Y.C., Abdelaziz, M.A., Tzeng, Y.S., Shih, A.C., Chen, S.Y., Yang, S.B., and Chen, C.C. (2024). Separate anterior paraventricular thalamus projections differentially regulate sensory and affective aspects of pain. Cell Rep *43*, 114946. 10.1016/j.celrep.2024.114946.
24. Liang, S.H., Zhao, W.J., Yin, J.B., Chen, Y.B., Li, J.N., Feng, B., Lu, Y.C., Wang, J., Dong, Y.L., and Li, Y.Q. (2020). A Neural Circuit from Thalamic Paraventricular Nucleus to Central Amygdala for the Facilitation of Neuropathic Pain. J Neurosci *40*, 7837-7854. 10.1523/JNEUROSCI.2487-19.2020.
25. Chang, Y.T., Chen, W.H., Shih, H.C., Min, M.Y., Shyu, B.C., and Chen, C.C. (2019). Anterior nucleus of paraventricular thalamus mediates chronic mechanical hyperalgesia. Pain *160*, 1208-1223. 10.1097/j.pain.0000000000001497.
26. Beas, B.S., Wright, B.J., Skirzewski, M., Leng, Y., Hyun, J.H., Koita, O., Ringelberg, N., Kwon, H.B., Buonanno, A., and Penzo, M.A. (2018). The locus coeruleus drives disinhibition in the midline thalamus via a dopaminergic mechanism. Nat Neurosci *21*, 963-973. 10.1038/s41593-018-0167-4.
27. Wang, Z., Wang, Z., and Zhou, Q. (2024). Modulation of learning safety signals by acute stress: paraventricular thalamus and prefrontal inhibition. Neuropsychopharmacology *49*, 961-973. 10.1038/s41386-023-01790-2.
28. Bhatnagar, S., and Corbett, B. (2017). Paraventricular Thalamic Regulation of Habituation to Repeated Stress: Molecular and Network Mechanisms. (NATURE PUBLISHING GROUP MACMILLAN BUILDING, 4 CRINAN ST, LONDON N1 9XW, ENGLAND), pp. S557-S558.
29. Beas, S., Gu, X., Leng, Y., Koita, O., Rodriguez-Gonzalez, S., Kindel, M., Matikainen-Ankney, B.A., Larsen, R.S., Kravitz, A.V., Hoon, M.A., and Penzo, M.A. (2020). A ventrolateral medulla-midline thalamic circuit for hypoglycemic feeding. Nat Commun *11*, 6218. 10.1038/s41467-020-19980-7.
30. Otis, J.M., Zhu, M., Namboodiri, V.M.K., Cook, C.A., Kosyk, O., Matan, A.M., Ying, R., Hashikawa, Y., Hashikawa, K., Trujillo-Pisanty, I., et al. (2019). Paraventricular Thalamus Projection Neurons Integrate Cortical and Hypothalamic Signals for Cue-Reward Processing. Neuron *103*, 423-431 e424. 10.1016/j.neuron.2019.05.018.

31. Do-Monte, F.H., Minier-Toribio, A., Quinones-Laracuente, K., Medina-Colon, E.M., and Quirk, G.J. (2017). Thalamic Regulation of Sucrose Seeking during Unexpected Reward Omission. Neuron *94*, 388-400 e384. 10.1016/j.neuron.2017.03.036.
32. Campus, P., Covelo, I.R., Kim, Y., Parsegian, A., Kuhn, B.N., Lopez, S.A., Neumaier, J.F., Ferguson, S.M., Solberg Woods, L.C., Sarter, M., and Flagel, S.B. (2019). The paraventricular thalamus is a critical mediator of top-down control of cue-motivated behavior in rats. Elife *8*. 10.7554/eLife.49041.
33. Do-Monte, F.H., Quinones-Laracuente, K., and Quirk, G.J. (2015). A temporal shift in the circuits mediating retrieval of fear memory. Nature *519*, 460-463. 10.1038/nature14030.
34. Quinones-Laracuente, K., Vega-Medina, A., and Quirk, G.J. (2021). Time-Dependent Recruitment of Prelimbic Prefrontal Circuits for Retrieval of Fear Memory. Front Behav Neurosci *15*, 665116. 10.3389/fnbeh.2021.665116.
35. Penzo, M.A., Robert, V., Tucciarone, J., De Bundel, D., Wang, M., Van Aelst, L., Darvas, M., Parada, L.F., Palmiter, R.D., He, M., et al. (2015). The paraventricular thalamus controls a central amygdala fear circuit. Nature *519*, 455-459. 10.1038/nature13978.
36. Paniccia, J.E., Vollmer, K.M., Green, L.M., Grant, R.I., Winston, K.T., Buchmaier, S., Westphal, A.M., Clarke, R.E., Doncheck, E.M., Bordieanu, B., et al. (2023). Restoration of a paraventricular thalamo-accumbal behavioral suppression circuit prevents reinstatement of heroin seeking. Neuron. 10.1016/j.neuron.2023.11.024.
37. Gao, C., Leng, Y., Ma, J., Rooke, V., Rodriguez-Gonzalez, S., Ramakrishnan, C., Deisseroth, K., and Penzo, M.A. (2020). Two genetically, anatomically and functionally distinct cell types segregate across anteroposterior axis of paraventricular thalamus. Nat Neurosci *23*, 217-228. 10.1038/s41593-019-0572-3.
38. Gao, C., Gohel, C.A., Leng, Y., Ma, J., Goldman, D., Levine, A.J., and Penzo, M.A. (2023). Molecular and spatial profiling of the paraventricular nucleus of the thalamus. Elife *12*. 10.7554/eLife.81818.
39. Beas, S., Khan, I., Gao, C., Loewinger, G., Macdonald, E., Bashford, A., Rodriguez-Gonzalez, S., Pereira, F., and Penzo, M.A. (2024). Dissociable encoding of motivated behavior by parallel thalamo-striatal projections. Curr Biol *34*, 1549-1560 e1543. 10.1016/j.cub.2024.02.037.
40. Loewinger, G., Cui, E., Lovinger, D., and Pereira, F. (2023). A Statistical Framework for Analysis of Trial-Level Temporal Dynamics in Fiber Photometry Experiments. bioRxiv. 10.1101/2023.11.06.565896.
41. Cui, E., Leroux, A., Smirnova, E., and Crainiceanu, C.M. (2022). Fast Univariate Inference for Longitudinal Functional Models. J Comput Graph Stat *31*, 219-230. 10.1080/10618600.2021.1950006.
42. Fujimoto, A., Murray, E.A., and Rudebeck, P.H. (2021). Interaction between decision-making and interoceptive representations of bodily arousal in frontal cortex. Proc Natl Acad Sci U S A *118*. 10.1073/pnas.2014781118.
43. Zhang, X., and van den Pol, A.N. (2017). Rapid binge-like eating and body weight gain driven by zona incerta GABA neuron activation. Science *356*, 853-859. 10.1126/science.aam7100.
44. Zhang, J., Chen, D., Sweeney, P., and Yang, Y. (2020). An excitatory ventromedial hypothalamus to paraventricular thalamus circuit that suppresses food intake. Nat Commun *11*, 6326. 10.1038/s41467-020-20093-4.
45. Ye, Q., Nunez, J., and Zhang, X. (2022). Oxytocin Receptor-Expressing Neurons in the Paraventricular Thalamus Regulate Feeding Motivation through Excitatory Projections to the Nucleus Accumbens Core. J Neurosci *42*, 3949-3964. 10.1523/JNEUROSCI.2042-21.2022.

46. Ong, Z.Y., Liu, J.J., Pang, Z.P., and Grill, H.J. (2017). Paraventricular Thalamic Control of Food Intake and Reward: Role of Glucagon-Like Peptide-1 Receptor Signaling. Neuropsychopharmacology *42*, 2387-2397. 10.1038/npp.2017.150.
47. Kessler, S., Labouebe, G., Croizier, S., Gaspari, S., Tarussio, D., and Thorens, B. (2021). Glucokinase neurons of the paraventricular nucleus of the thalamus sense glucose and decrease food consumption. iScience *24*, 103122. 10.1016/j.isci.2021.103122.
48. Cheng, J., Wang, J., Ma, X., Ullah, R., Shen, Y., and Zhou, Y.D. (2018). Anterior Paraventricular Thalamus to Nucleus Accumbens Projection Is Involved in Feeding Behavior in a Novel Environment. Front Mol Neurosci *11*, 202. 10.3389/fnmol.2018.00202.
49. Livneh, Y., Sugden, A.U., Madara, J.C., Essner, R.A., Flores, V.I., Sugden, L.A., Resch, J.M., Lowell, B.B., and Andermann, M.L. (2020). Estimation of Current and Future Physiological States in Insular Cortex. Neuron *105*, 1094-1111 e1010. 10.1016/j.neuron.2019.12.027.
50. R, G.A., Campbell, E.J., Walker, L.C., S, S.C.n., Muthmainah, M., F, S.K., A, M.G., O'Shea, M.J., He, S., Dayas, C.V., et al. (2023). A paraventricular thalamus to insular cortex glutamatergic projection gates "emotional" stress-induced binge eating in females. Neuropsychopharmacology *48*, 1931-1940. 10.1038/s41386-023-01665-6.
51. Yun-Qing Li, J.-N.L., Liu-Jie Zhao et al. (2025). Central Recruitment mechanism of Itch and Pain Through the Paraventricular Thalamic Nucleus in a Pathway- and Intensity-Dependent Manner. Research Square PREPRINT https://doi.org/10.21203/rs.3.rs-5615052/v1.
52. Li, J.N., Wu, X.M., Zhao, L.J., Sun, H.X., Hong, J., Wu, F.L., Chen, S.H., Chen, T., Li, H., Dong, Y.L., and Li, Y.Q. (2023). Central medial thalamic nucleus dynamically participates in acute itch sensation and chronic itch-induced anxiety-like behavior in male mice. Nat Commun *14*, 2539. 10.1038/s41467-023-38264-4.
53. Dong, X., Li, Y., and Kirouac, G.J. (2015). Blocking of orexin receptors in the paraventricular nucleus of the thalamus has no effect on the expression of conditioned fear in rats. Front Behav Neurosci *9*, 161. 10.3389/fnbeh.2015.00161.
54. Dong, X., Li, S., and Kirouac, G.J. (2020). A projection from the paraventricular nucleus of the thalamus to the shell of the nucleus accumbens contributes to footshock stress-induced social avoidance. Neurobiol Stress *13*, 100266. 10.1016/j.ynstr.2020.100266.
55. Kooiker, C.L., Birnie, M.T., and Baram, T.Z. (2021). The Paraventricular Thalamus: A Potential Sensor and Integrator of Emotionally Salient Early-Life Experiences. Front Behav Neurosci *15*, 673162. 10.3389/fnbeh.2021.673162.
56. Ren, S., Wang, Y., Yue, F., Cheng, X., Dang, R., Qiao, Q., Sun, X., Li, X., Jiang, Q., Yao, J., et al. (2018). The paraventricular thalamus is a critical thalamic area for wakefulness. Science *362*, 429-434. 10.1126/science.aat2512.
57. Hua, R., Wang, X., Chen, X., Wang, X., Huang, P., Li, P., Mei, W., and Li, H. (2018). Calretinin Neurons in the Midline Thalamus Modulate Starvation-Induced Arousal. Curr Biol *28*, 3948-3959 e3944. 10.1016/j.cub.2018.11.020.
58. Zhu, Y., Nachtrab, G., Keyes, P.C., Allen, W.E., Luo, L., and Chen, X. (2018). Dynamic salience processing in paraventricular thalamus gates associative learning. Science *362*, 423-429. 10.1126/science.aat0481.
59. Kelley, A.E., Baldo, B.A., and Pratt, W.E. (2005). A proposed hypothalamic-thalamic-striatal axis for the integration of energy balance, arousal, and food reward. J Comp Neurol *493*, 72-85. 10.1002/cne.20769.
60. Iglesias, A.G., and Flagel, S.B. (2021). The Paraventricular Thalamus as a Critical Node of Motivated Behavior via the Hypothalamic-Thalamic-Striatal Circuit. Front Integr Neurosci *15*, 706713. 10.3389/fnint.2021.706713.

61. Curtis, G.R., Oakes, K., and Barson, J.R. (2020). Expression and Distribution of Neuropeptide-Expressing Cells Throughout the Rodent Paraventricular Nucleus of the Thalamus. Front Behav Neurosci *14*, 634163. 10.3389/fnbeh.2020.634163.
62. Labouebe, G., Boutrel, B., Tarussio, D., and Thorens, B. (2016). Glucose-responsive neurons of the paraventricular thalamus control sucrose-seeking behavior. Nat Neurosci *19*, 999-1002. 10.1038/nn.4331.
63. Kolaj, M., Zhang, L., Ronnekleiv, O.K., and Renaud, L.P. (2012). Midline thalamic paraventricular nucleus neurons display diurnal variation in resting membrane potentials, conductances, and firing patterns in vitro. J Neurophysiol *107*, 1835-1844. 10.1152/jn.00974.2011.
64. Engelke, D.S., Zhang, X.O., O'Malley, J.J., Fernandez-Leon, J.A., Li, S., Kirouac, G.J., Beierlein, M., and Do-Monte, F.H. (2021). A hypothalamic-thalamostriatal circuit that controls approach-avoidance conflict in rats. Nat Commun *12*, 2517. 10.1038/s41467-021-22730-y.
65. van Opstal, A.M., Kaal, I., van den Berg-Huysmans, A.A., Hoeksma, M., Blonk, C., Pijl, H., Rombouts, S., and van der Grond, J. (2019). Dietary sugars and non-caloric sweeteners elicit different homeostatic and hedonic responses in the brain. Nutrition *60*, 80-86. 10.1016/j.nut.2018.09.004.
66. Frank, G.K., Oberndorfer, T.A., Simmons, A.N., Paulus, M.P., Fudge, J.L., Yang, T.T., and Kaye, W.H. (2008). Sucrose activates human taste pathways differently from artificial sweetener. Neuroimage *39*, 1559-1569. 10.1016/j.neuroimage.2007.10.061.
67. Low, Y.Q., Lacy, K., and Keast, R. (2014). The role of sweet taste in satiation and satiety. Nutrients *6*, 3431-3450. 10.3390/nu6093431.
68. Zhang, L., Koller, J., Ip, C.K., Gopalasingam, G., Bajaj, N., Lee, N.J., Enriquez, R.F., and Herzog, H. (2021). Lack of neuropeptide FF signalling in mice leads to reduced repetitive behavior, altered drinking behavior, and fuel type selection. FASEB J *35*, e21980. 10.1096/fj.202100703R.
69. Akash, G., Changwoo, S., Ryan, J.P., Durga, S.K., Julia, A.S., and Melissa, R.W. (2020). Ramping activity in midbrain dopamine neurons signifies the use of a cognitive map. bioRxiv, 2020.2005.2021.108886. 10.1101/2020.05.21.108886.
70. Wang, X., Wu, Q., Egan, L., Gu, X., Liu, P., Gu, H., Yang, Y., Luo, J., Wu, Y., Gao, Z., and Fan, J. (2019). Anterior insular cortex plays a critical role in interoceptive attention. Elife *8*. 10.7554/eLife.42265.
71. Takemoto, M., Kato, S., Kobayashi, K., and Song, W.J. (2023). Dissection of insular cortex layer 5 reveals two sublayers with opposing modulatory roles in appetitive drinking behavior. iScience *26*, 106985. 10.1016/j.isci.2023.106985.
72. Herman, J.P., McKlveen, J.M., Ghosal, S., Kopp, B., Wulsin, A., Makinson, R., Scheimann, J., and Myers, B. (2016). Regulation of the Hypothalamic-Pituitary-Adrenocortical Stress Response. Compr Physiol *6*, 603-621. 10.1002/cphy.c150015.
73. Herman, J.P. (2013). Neural control of chronic stress adaptation. Front Behav Neurosci *7*, 61. 10.3389/fnbeh.2013.00061.
74. He, Y., Ren, Y., Chen, X., Wang, Y., Yu, H., Cai, J., Wang, P., Ren, Y., and Xie, P. (2024). Neural and molecular investigation into the paraventricular thalamus for chronic restraint stress induced depressive-like behaviors. J Adv Res. 10.1016/j.jare.2024.10.025.
75. Cui, L., Li, S., Wang, S., Wu, X., Liu, Y., Yu, W., Wang, Y., Tang, Y., Xia, M., and Li, B. (2024). Major depressive disorder: hypothesis, mechanism, prevention and treatment. Signal Transduct Target Ther *9*, 30. 10.1038/s41392-024-01738-y.
76. Cao, Y., Wu, Z., Zhang, M., Ji, R., Zhang, H., and Song, L. (2024). Microglial adenosine A(2A) receptor in the paraventricular thalamic nucleus regulates pain sensation and analgesic effects independent of opioid and cannabinoid receptors. Front Pharmacol *15*, 1467305. 10.3389/fphar.2024.1467305.

77. Chang, J., Li, Z., Yuan, H., Wang, X., Xu, J., Yang, P., and Qin, L. (2024). Protective role of aconitate decarboxylase 1 in neuroinflammation-induced dysfunctions of the paraventricular thalamus and sleepiness. Commun Biol *7*, 1484. 10.1038/s42003-024-07215-0.
78. Cheng, J., Ma, X., Li, C., Ullah, R., Wang, X., Long, J., Yuan, Z., Liu, S., Fu, J., Chen, Z., et al. (2022). Diet-induced inflammation in the anterior paraventricular thalamus induces compulsive sucrose-seeking. Nat Neurosci *25*, 1009-1013. 10.1038/s41593-022-01129-y.
79. Kasahara, T., Takata, A., Kato, T.M., Kubota-Sakashita, M., Sawada, T., Kakita, A., Mizukami, H., Kaneda, D., Ozawa, K., and Kato, T. (2016). Depression-like episodes in mice harboring mtDNA deletions in paraventricular thalamus. Mol Psychiatry *21*, 39-48. 10.1038/mp.2015.156.
80. Flagel, S.B. (2022). The paraventricular nucleus of the thalamus and its potential role in psychopathology. Neuropsychopharmacology *47*, 385-386. 10.1038/s41386-021-01112-4.
81. Marcus, D.J., English, A.E., Chun, G., Seth, E.F., Oomen, R., Hwang, S., Wells, B., Piantadosi, S.C., Suko, A., Li, Y., et al. (2025). Endocannabinoids facilitate transitory reward engagement through retrograde gain-control. bioRxiv. 10.1101/2025.01.06.630792.
82. Shima, Y., Skibbe, H., Sasagawa, Y., Fujimori, N., Iwayama, Y., Isomura-Matoba, A., Yano, M., Ichikawa, T., Nikaido, I., Hattori, N., and Kato, T. (2023). Distinctiveness and continuity in transcriptome and connectivity in the anterior-posterior axis of the paraventricular nucleus of the thalamus. Cell Rep *42*, 113309. 10.1016/j.celrep.2023.113309.

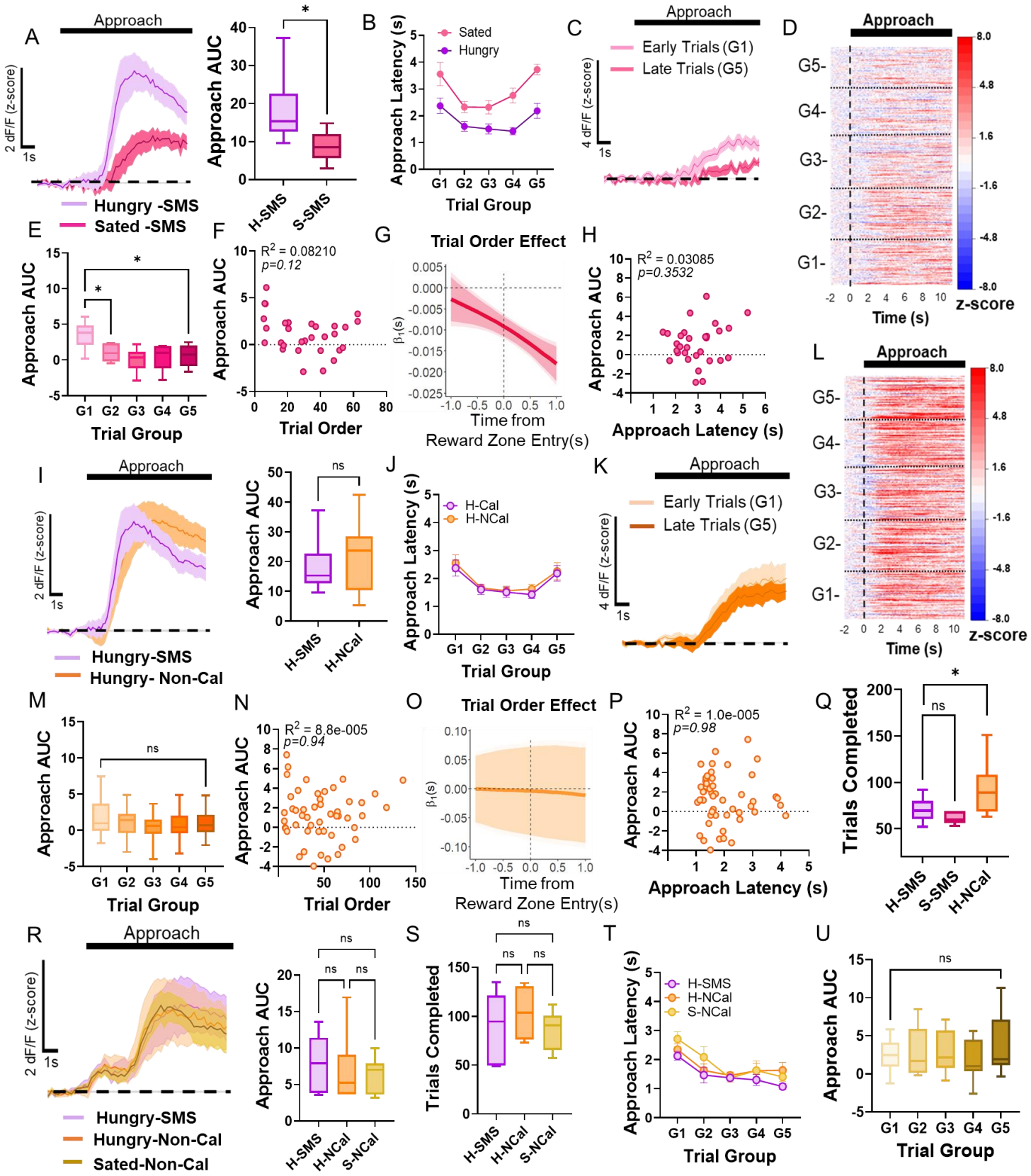
A
Approach
2 dF/F (z-score)
1s
Hungry -SMS
Sated -SMS
Approach AUC
H-SMS
S-SMS
B
Sated
Hungry
Approach Latency (s)
Trial Group
C
Approach
Early Trials (G1)
Late Trials (G5)
4 dF/F (z-score)
D
Approach
G5-
G4-
G3-
G2-
G1-
Time (s)
z-score
E
Approach AUC
Trial Group
F
R^2 = 0.08210
p=0.12
Trial Order
G
Trial Order Effect
β_1(s)
Time from
Reward Zone Entry(s)
H
R^2 = 0.03085
p=0.3532
Approach Latency (s)
L
Approach
I
Hungry-SMS
Hungry- Non-Cal
ns
J
H-Cal
H-NCal
K
Early Trials (G1)
Late Trials (G5)
M
N
R^2 = 8.8e-005
p=0.94
O
P
R^2 = 1.0e-005
p=0.98
Q
Trials Completed
R
Hungry-SMS
Hungry-Non-Cal
Sated-Non-Cal
S
T
H-SMS
H-NCal
S-NCal
U

Figure 1

FIGURE LEGENDS

Figure 1. PVT^{D2+} neuronal activity state-dependent modulation is contingent on calorie intake.

(A) Average GCaMP6s responses from PVT^{D2+} neurons and AUC quantification showing comparisons between ramping activity during reward approach in test session where hungry mice were given a SMS reward (H-SMS) and sessions where sated mice were given a SMS reward (S-SMS). S-SMS: n = 368 trials from 5 mice, comparisons between H-SMS approach and S-SMS approach; Two-tailed unpaired t-test *$p<0.05$. **(B)** Latencies to reach the reward zone across 'trial group blocks' (G1 – G5) for H-SMS and S-SMS sessions. Two-way ANOVA, Effect of trial group block****$p<0.0001$; Effect of test session (satiety) ****$p<0.0001$; Interaction $p=0.46$; ns, not significant. **(C)** Average GCaMP6s responses from PVT^{D2+} neurons comparing reward approach between early 'G1' and late 'G5' trials within the sated-SMS test sessions. **(D)** Heatmap showing reward approach responses from PVT^{D2+} neurons during sated-SMS test sessions, time-locked to approach onset, sorted by trial order, and binned into 5 'trial group blocks' (G1 – G5). **(E)** AUC quantification of the reward approach-evoked changes in GCaMP6s activity across trial group blocks within the sated-SMS test sessions. Repeated measures ANOVA, **$p<0.001$. G1 vs. G2 Dunnett's multiple comparisons test *$p<0.05$. G1 vs. G5 Dunnett's multiple comparisons test *$p<0.05$. **(F)** Correlation between the AUC of the reward approach-evoked changes in GCaMP6s activity and trial order within the sated-SMS test session. **(G)** FLMM coefficient estimates plots of the approach trial order effect and statistical significance at each trial time-point results for the photometric responses of PVT^{D2+} neurons for reward zone entry. The plot shows a negative association between PVT^{D2+} GCaMP6s responses and trial order before and after reward zone entry for the S-SMS test session. **(H)** No correlation between the AUC of the reward approach-evoked changes in GCaMP6s activity and approach latency within the S-SMS test session. **(I)** Average GCaMP6s responses from PVT^{D2+}

1075 neurons and AUC quantification showing comparisons between ramping activity during reward
1076 approach in test session where hungry mice were given a SMS reward (H-SMS) and sessions
1077 where hungry mice were given a sweet non-caloric reward (H-NCal). H-NCal: n = 928 trials from
1078 5 mice, comparisons between H-SMS approach and H-NCal approach; Two-tailed unpaired t-
1079 test *p=0.40*; ns, not significant. **(J)** Latencies to reach the reward zone across 'trial group blocks'
1080 (G1 – G5) for H-SMS and H-NCal sessions. Two-way ANOVA, Effect of trial group
1081 block****$p<0.0001$; Effect of test session (Caloric vs. Non-Caloric) *p=0.44;* Interaction *p=0.99*;
1082 ns, not significant. **(K)** Average GCaMP6s responses from PVT^{D2+} neurons comparing reward
1083 approach between early 'G1' and late 'G5' trials within the H-NCal test sessions. **(L)** Heatmap
1084 showing reward approach responses from PVT^{D2+} neurons during H-NCal test sessions, time-
1085 locked to approach onset, sorted by trial order, and binned into 5 'trial group blocks' (G1 – G5).
1086 **(M)** AUC quantification of the reward approach-evoked changes in GCaMP6s activity across
1087 trial group blocks within the H-NCal test sessions. Repeated measures ANOVA, *p=0.078*. G1 vs.
1088 G5 Dunnett's multiple comparisons test *p=0.43;* ns, not significant. **(N)** No correlation between
1089 the AUC of the reward approach-evoked changes in GCaMP6s activity and trial order within the
1090 H-NCal test sessions. **(O)** FLMM coefficient estimates plots of the approach trial order effect and
1091 statistical significance at each trial time-point results for the photometric responses of PVT^{D2+}
1092 neurons for reward zone entry. The plot shows no significant association between PVT^{D2+}
1093 GCaMP6s responses and trial order for the H-NCal test sessions. **(P)** No correlation between
1094 the AUC of the reward approach-evoked changes in GCaMP6s activity and approach latency
1095 within the H-NCal test sessions. **(Q)** Quantification of trials completed within a session
1096 comparing trials during the H-SMS, the S-SMS and the H-NCal test sessions. H-SMS vs. S-
1097 SMS: Two-tailed unpaired t-test *p=0.12*; ns, not significant. H-SMS vs. H-NCal: Two-tailed
1098 unpaired t-test *$p<0.05$. **(R)** Average GCaMP6s responses from PVT^{D2+} neurons and AUC
1099 quantification showing comparisons between ramping activity during reward approach in test
1100 session where hungry mice were given a SMS reward (H-SMS), sessions where hungry mice

1101 were given a sweet non-caloric reward (H-NCal), and sessions where sated mice were given
1102 the non-caloric reward (S-NCal). H-SMS: n = 540 trials, H-NCal: n= 414 trials and S-NCal: 515
1103 trials from 4 mice. Repeated measures ANOVA, *p=0.86;* ns, not significant. **(S)** Quantification of
1104 trials completed within a session comparing trials during the H-SMS, the H-NCal and the S-NCal
1105 test sessions. Repeated measures ANOVA, *p=0.64;* ns, not significant. **(T)** Latencies to reach
1106 the reward zone across 'trial group blocks' (G1 – G5) for H-SMS, H-NCal, S-NCal sessions.
1107 Two-way ANOVA, Effect of trial group block****$p<0.0001$; Effect of test session *$p<0.05$;
1108 Interaction $p=0.82$ ns, not significant. **(U)** AUC quantification of the reward approach-evoked
1109 changes in GCaMP6s activity across trial group blocks within the S-NCal test sessions.
1110 Repeated measures ANOVA, *p=0.83;* ns, not significant.

1111

1112

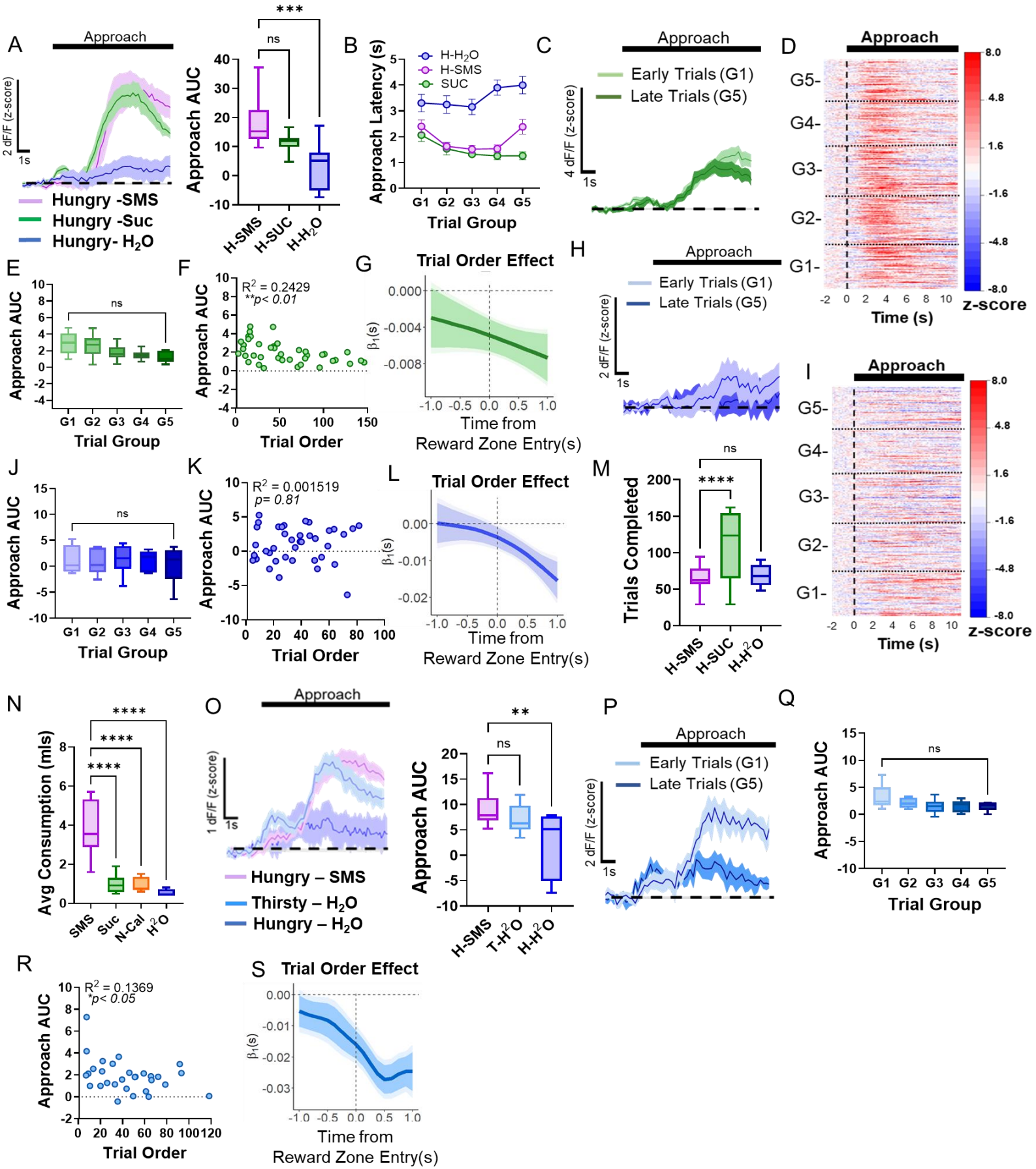
A
Approach
2 dF/F (z-score)
1s
Hungry -SMS
Hungry -Suc
Hungry- H2O
Approach AUC
***
ns
H-SMS
H-SUC
H-H2O
B
Approach Latency (s)
H-H2O
H-SMS
SUC
G1 G2 G3 G4 G5
Trial Group
C
Approach
Early Trials (G1)
Late Trials (G5)
4 dF/F (z-score)
1s
D
Approach
G5-
G4-
G3-
G2-
G1-
Time (s)
z-score
E
Approach AUC
ns
G1 G2 G3 G4 G5
Trial Group
F
R2 = 0.2429
**p< 0.01
Approach AUC
Trial Order
G
Trial Order Effect
β1(s)
Time from
Reward Zone Entry(s)
H
Approach
Early Trials (G1)
Late Trials (G5)
2 dF/F (z-score)
1s
I
Approach
G5-
G4-
G3-
G2-
G1-
Time (s)
z-score
J
Approach AUC
ns
G1 G2 G3 G4 G5
Trial Group
K
R2 = 0.001519
p= 0.81
Approach AUC
Trial Order
L
Trial Order Effect
β1(s)
Time from
Reward Zone Entry(s)
M
Trials Completed
ns
****
H-SMS
H-SUC
H-H2O
N
Avg Consumption (mls)
****
****
****
SMS
Suc
N-Cal
H2O
O
Approach
1 dF/F (z-score)
1s
Hungry – SMS
Thirsty – H2O
Hungry – H2O
Approach AUC
**
ns
H-SMS
T-H2O
H-H2O
P
Approach
Early Trials (G1)
Late Trials (G5)
2 dF/F (z-score)
1s
Q
Approach AUC
ns
G1 G2 G3 G4 G5
Trial Group
R
R2 = 0.1369
*p< 0.05
Approach AUC
Trial Order
S
Trial Order Effect
β1(s)
Time from
Reward Zone Entry(s)

Figure 2

Figure 2. PVT^{D2+} neuronal activity is modulated by the interoceptive value of the outcome.

(A) Average GCaMP6s responses from PVT^{D2+} neurons and AUC quantification showing comparisons between ramping activity during reward approach in test session where hungry mice were given a SMS reward (H-SMS), sessions where hungry mice were given a 10% sucrose solution (H-Suc), and sessions where hungry mice were given water (H- H_2O). H-SMS: n = 460 trials, H-Suc: n= 885 trials and H- H_2O: 549 trials from 4 mice. Repeated measures ANOVA, ***p<0.01*. H-SMS vs. H-Suc Dunnett's multiple comparisons test *p=0.12;* ns, not significant. H-SMS vs. H- H_2O Dunnett's multiple comparisons test ****p<0.001*. **(B)** Latencies to reach the reward zone across 'trial group blocks' (G1 – G5) for H-SMS, H-Suc, H-H_2O sessions. Two-way ANOVA, Effect of trial group block**p<0.05*; Effect of test session *****p<0.0001;* Interaction **p<0.05*. **(C)** Average GCaMP6s responses from PVT^{D2+} neurons comparing reward approach between early 'G1' and late 'G5' trials within the H-Suc test sessions. **(D)** Heatmap showing reward approach responses from PVT^{D2+} neurons during H-Suc test sessions, time-locked to approach onset, sorted by trial order, and binned into 5 'trial group blocks' (G1 – G5). **(E)** AUC quantification of the reward approach-evoked changes in GCaMP6s activity across trial group blocks within the H-Suc test sessions. Repeated measures ANOVA, ***p<0.001*. G1 vs. G2 Dunnett's multiple comparisons test **p<0.05*. G1 vs. G5 Dunnett's multiple comparisons test **p<0.05*. **(F)** Correlation between the AUC of the reward approach-evoked changes in GCaMP6s activity and trial order within the H-Suc test sessions. **(G)** FLMM coefficient estimates plots of the approach trial order effect and statistical significance at each trial time-point results for the photometric responses of PVT^{D2+} neurons for reward zone entry. The plot shows a negative association between PVT^{D2+} GCaMP6s responses and trial order before and after reward zone entry for the H-Suc test sessions. **(H)** Average GCaMP6s responses from PVT^{D2+} neurons comparing reward approach between early 'G1' and late 'G5' trials within the hungry-H_2O test sessions. **(I)** Heatmap showing reward approach responses from PVT^{D2+} neurons

during hungry- H_2O test sessions, time-locked to approach onset, sorted by trial order, and binned into 5 'trial group blocks' (G1 – G5). **(J)** AUC quantification of the reward approach-evoked changes in GCaMP6s activity across trial group blocks within the H-H_2O test sessions. Repeated measures ANOVA, *p=0.50* ns, not significant. **(K)** Correlation between the AUC of the reward approach-evoked changes in GCaMP6s activity and trial order within the H-H_2O test sessions. **(L)** FLMM coefficient estimates plots of the approach trial order effect and statistical significance at each trial time-point results for the photometric responses of PVT^{D2+} neurons for reward zone entry. The plot shows a negative association between PVT^{D2+} GCaMP6s responses and trial order only after reward zone entry for the H-H_2O test sessions. **(M)** Quantification of trials completed within a session comparing trials performed during the H-SMS, the H-Suc, and the H-H_2O test sessions. Repeated measures ANOVA, ****$p<0.0001$. H-SMS vs. H-Suc Dunnett's multiple comparisons test ****$p<0.0001$. H-SMS vs. H-H^2O Dunnett's multiple comparisons test *p=0.95* ns, not significant. **(N)** Quantification of average consumption (mls) in a 4-bottle test of SMS, 10% Suc, Non-Cal and H-H_2O ad libitum consumption. Repeated measures ANOVA, ****$p<0.0001$. **(O)** Average GCaMP6s responses from PVT^{D2+} neurons and AUC quantification showing comparisons between ramping activity during reward approach in test session where hungry mice were given a SMS reward (H-SMS), sessions where thirsty mice were given water (T-H_2O), and sessions where hungry mice were given water (H-H^2O). H-SMS: n = 1111 trials, T-H_2O: n= 605 trials and H-H_2O: 458 trials from 4 mice. Repeated measures ANOVA, **$p<0.01$. H-SMS vs. T-H_2O Dunnett's multiple comparisons test *p=0.58;* ns, not significant. H-SMS vs. H-H^2O Dunnett's multiple comparisons test **$p<0.01$. **(P)** Average GCaMP6s responses from PVT^{D2+} neurons comparing reward approach between early 'G1' and late 'G5' trials within the T-H^2O test sessions. **(Q)** AUC quantification of the reward approach-evoked changes in GCaMP6s activity across trial group blocks within the T-H_2O test sessions. Repeated measures ANOVA, *p=0.17*. G1 vs. G5 Dunnett's multiple comparisons test *p=0.40;*

ns, not significant. **(R)** Correlation between the AUC of the reward approach-evoked changes in GCaMP6s activity and trial order within the T-H_2O test sessions.

(S) FLMM coefficient estimates plots of the approach trial order effect and statistical significance at each trial time-point results for the photometric responses of PVT^{D2+} neurons for reward zone entry. The plot shows a negative association between PVT^{D2+} GCaMP6s responses and trial order before and after reward zone entry for the T-H_2O test sessions.

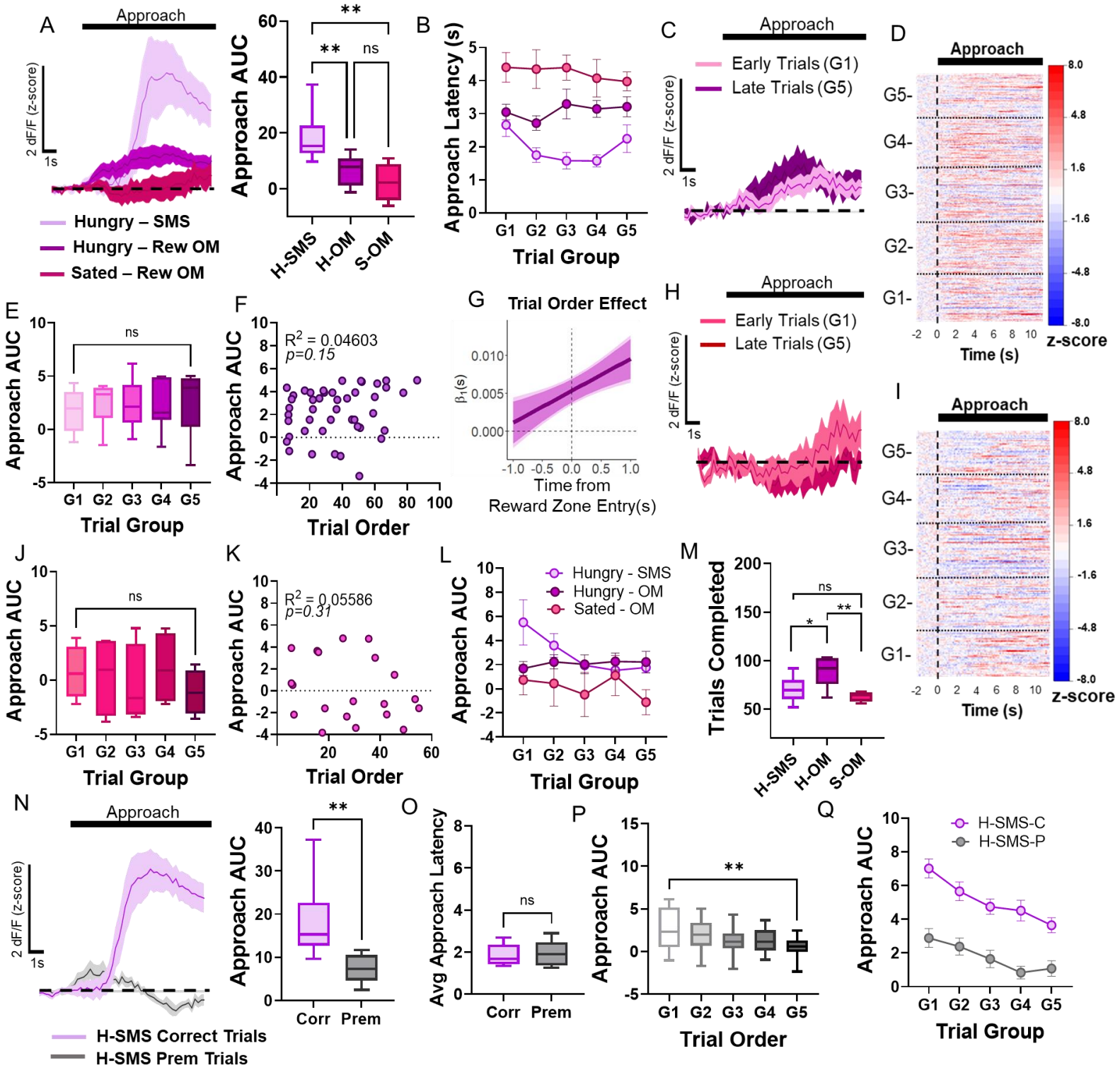
A
Approach
2 dF/F (z-score)
1s
Hungry – SMS
Hungry – Rew OM
Sated – Rew OM
Approach AUC
**
**
ns
H-SMS
H-OM
S-OM
B
Approach Latency (s)
G1 G2 G3 G4 G5
Trial Group
C
Approach
Early Trials (G1)
Late Trials (G5)
2 dF/F (z-score)
1s
D
Approach
G5-
G4-
G3-
G2-
G1-
Time (s)
z-score
E
Approach AUC
ns
G1 G2 G3 G4 G5
Trial Group
F
Approach AUC
R^2 = 0.04603
p=0.15
Trial Order
G
Trial Order Effect
β_1(s)
Time from
Reward Zone Entry(s)
H
Approach
Early Trials (G1)
Late Trials (G5)
2 dF/F (z-score)
1s
I
Approach
G5-
G4-
G3-
G2-
G1-
Time (s)
z-score
J
Approach AUC
ns
G1 G2 G3 G4 G5
Trial Group
K
Approach AUC
R^2 = 0.05586
p=0.31
Trial Order
L
Approach AUC
Hungry - SMS
Hungry - OM
Sated - OM
G1 G2 G3 G4 G5
Trial Group
M
Trials Completed
ns
*
**
H-SMS
H-OM
S-OM
N
Approach
2 dF/F (z-score)
1s
H-SMS Correct Trials
H-SMS Prem Trials
Approach AUC
**
Corr Prem
O
Avg Approach Latency
ns
Corr Prem
P
Approach AUC
**
G1 G2 G3 G4 G5
Trial Order
Q
Approach AUC
H-SMS-C
H-SMS-P
G1 G2 G3 G4 G5
Trial Group

Figure 3

Figure 3. PVT^{D2+} neuronal activity is state and outcome dependent.

(A) Average GCaMP6s responses from PVT^{D2+} neurons and AUC quantification showing comparisons between ramping activity during reward approach after extensive training in the task for H-SMS test sessions, for sessions where hungry mice were not given a reward (H-OM), and sessions where sated mice were not given a reward (S-OM), H-SMS: n = 705 trials, H-OM: n= 797 trials and S-OM: 253 trials from 5 mice. Repeated measures ANOVA, ***$p<0.01$*. H-SMS vs. H-OM Tukey's multiple comparisons test ***$p<0.01$*. H-SMS vs. S-OM Tukey's multiple comparisons test ***$p<0.01$.* H-OM vs. S-OM Tukey's multiple comparisons test *$p=0.58$;* ns, not significant. **(B)** Latencies to reach the reward zone across 'trial group blocks' (G1 – G5) for H-SMS, H-OM, S-OM sessions. Two-way ANOVA, Effect of trial group block *$p=0.54$*; ns, not significant. Effect of test session ****$p<0.0001$;* Interaction *$p=0.44$* ns, not significant. **(C)** Average GCaMP6s responses from PVT^{D2+} neurons comparing reward approach between early 'G1' and late 'G5' trials within the H-OM test sessions. **(D)** Heatmap showing reward approach responses from PVT^{D2+} neurons during H-OM test sessions, time-locked to approach onset, sorted by trial order, and binned into 5 'trial group blocks' (G1 – G5).

(E) AUC quantification of the reward approach-evoked changes in GCaMP6s activity across trial group blocks within the H-OM test sessions. Repeated measures ANOVA *$p=0.45$* ns, not significant. **(F)** Correlation between the AUC of the reward approach-evoked changes in GCaMP6s activity and trial order within the H-OM test sessions. **(G)** FLMM coefficient estimates plots of the approach trial order effect and statistical significance at each trial time-point results for the photometric responses of PVT^{D2+} neurons for reward zone entry. The plot shows a positive association between PVT^{D2+} GCaMP6s responses and trial order before and after reward zone entry for the H-OM test sessions. **(H)** Average GCaMP6s responses from PVT^{D2+} neurons comparing reward approach between early 'G1' and late 'G5' trials within the S-OM test sessions. **(I)** Heatmap showing reward approach responses from PVT^{D2+} neurons during S-OM

test sessions, time-locked to approach onset, sorted by trial order, and binned into 5 'trial group blocks' (G1 – G5). **(J)** AUC quantification of the reward approach-evoked changes in GCaMP6s activity across trial group blocks within the S-OM test sessions. Repeated measures ANOVA, *p=0.45* ns, not significant. **(K)** No correlation between the AUC of the reward approach-evoked changes in GCaMP6s activity and trial order within the S-OM test sessions. **(L)** AUC quantification of the reward approach across 'trial group blocks' (G1 – G5) for H-SMS, H-OM, S-OM sessions. Two-way ANOVA, Effect of trial group block *p=0.26*; ns, not significant. Effect of test session ***p<0.01;* Interaction *p=0.27* ns, not significant. **(M)** Quantification of trials completed within a session comparing trials performed during the H-SMS, the H-OM and the S-OM test sessions. Repeated measures ANOVA, ***p<0.01.* H-SMS vs. H-OM Tukey's multiple comparisons test **p<0.05*. H-SMS vs. S-OM Tukey's multiple comparisons test *p=0.60* ns, not significant. H-OM vs. S-OM Tukey's multiple comparisons test ***p<0.01*. **(N)** Average GCaMP6s responses from PVT^{D2+} neurons and AUC quantification showing comparisons between ramping activity during reward approach in correct and premature trials in the H-SMS test sessions. Two-tailed paired t-test ***p<0.01*. **(O)** Latencies to reach the reward zone for correct and premature trials performed in the H-SMS test sessions. Two-tailed paired t-test *p=0.60* ns, not significant. **(P)** AUC quantification of the reward approach-evoked changes in GCaMP6s activity across trial group blocks for the H-SMS premature trials. Repeated measures ANOVA, ****p<0.001*. G1 vs. G5 Dunnett's multiple comparisons test ***p<0.01.* **(O)** AUC quantification of the reward approach across 'trial group blocks' (G1 – G5) for H-SMS-C (correct) and H-SMS-P (premature) trials. Two-way ANOVA, Effect of trial group block *****p<0.0001*. Effect of trial type *****p<0.0001;* Interaction *p=0.61* ns, not significant.

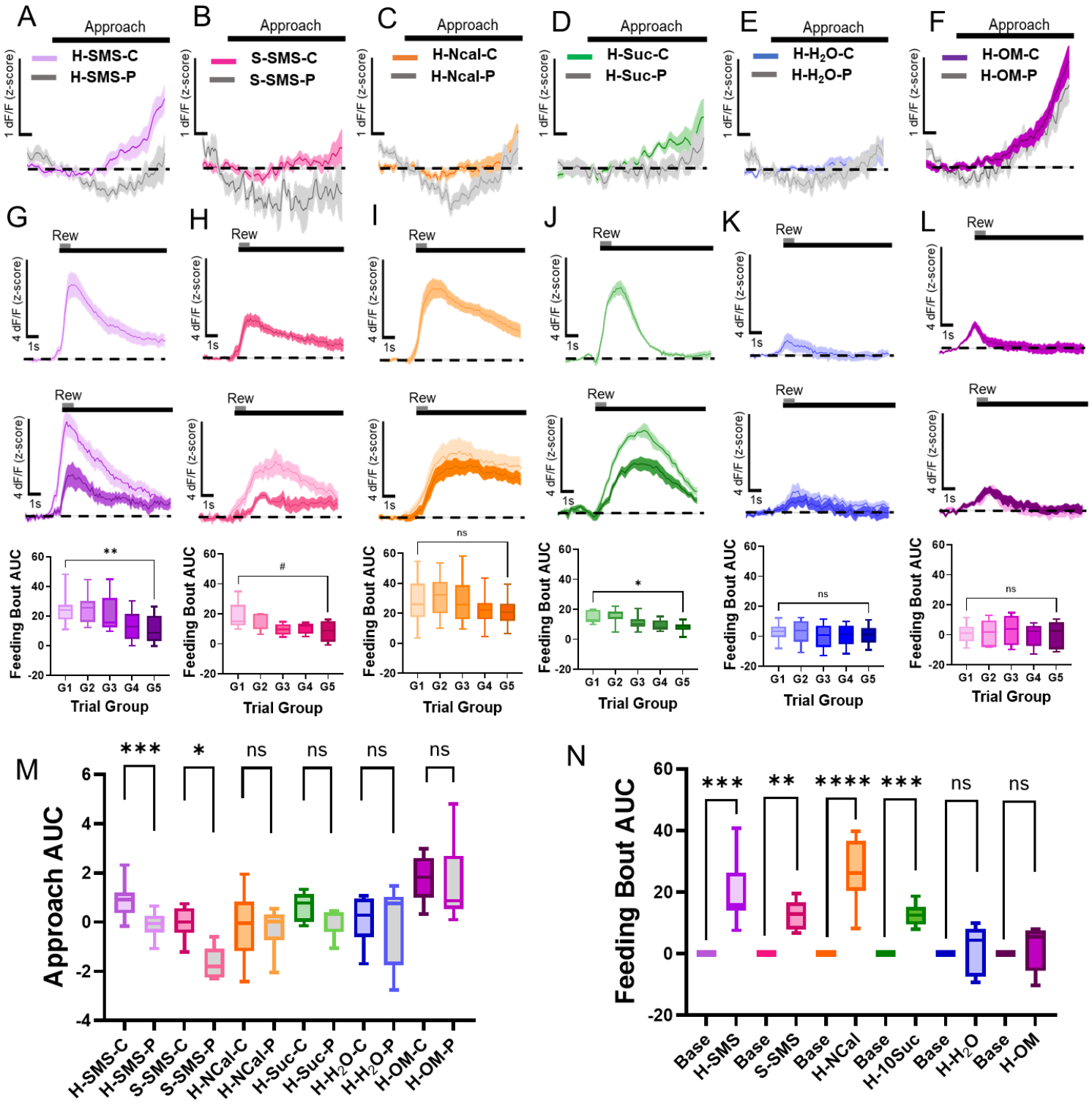
A
Approach
H-SMS-C
H-SMS-P
B
S-SMS-C
S-SMS-P
C
H-Ncal-C
H-Ncal-P
D
H-Suc-C
H-Suc-P
E
H-H2O-C
H-H2O-P
F
H-OM-C
H-OM-P
1 dF/F (z-score)
G
H
I
J
K
L
Rew
4 dF/F (z-score)
1s
Feeding Bout AUC
Trial Group
G1 G2 G3 G4 G5
**
#
ns
*
M
Approach AUC
H-SMS-C
H-SMS-P
S-SMS-C
S-SMS-P
H-NCal-C
H-NCal-P
H-Suc-C
H-Suc-P
H-H2O-C
H-H2O-P
H-OM-C
H-OM-P
N
Base
H-SMS
S-SMS
H-NCal
H-10Suc
H-H2O
H-OM

Figure 4

1220 **Figure 4. PVT^{D2+} neuronal activity during approach-only is modulated by outcome and**
1221 **outcome expectation.**

1222 **(A-F)** Average GCaMP6s responses from PVT^{D2+} neurons during approach only and
1223 normalized by linear interpolation showing comparisons between correct and premature trials in
1224 the H-SMS test sessions **(A)**, for S-SMS test sessions **(B)**, for H-NCal test sessions **(C)**, for H-
1225 Suc test sessions **(D),** for H-H_2O test sessions **(E),** and for H-OM test sessions **(F). (G-L)**
1226 Average GCaMP6s responses from PVT^{D2+} neurons (top), comparisons between early 'G1' and
1227 late 'G5' trials (middle) and AUC quantifications across trial groups (bottom) during reward
1228 delivery and feeding bouts for the **(G)** H-SMS test sessions; Repeated measures ANOVA,
1229 ****$p<0.0001$. G1 vs. G5 Dunnett's multiple comparisons test **$p<0.01$, **(H)** for S-SMS test
1230 sessions; Repeated measures ANOVA, $p=0.10$, *ns.* G1 vs. G5 Dunnett's multiple comparisons
1231 test $^{\#}p=0.07$, *ns*, **(I)** for H-NCal test sessions; Repeated measures ANOVA, $p=0.17$, *ns.* G1 vs.
1232 G5 Dunnett's multiple comparisons test $p=0.65$, *ns*, **(J)** for H-Suc test sessions; Repeated
1233 measures ANOVA, ***$p<0.001$. G1 vs. G5 Dunnett's multiple comparisons test *$p<0.05$, **(K)** for
1234 H-H_2O test sessions; Repeated measures ANOVA, $p=0.48$, *ns.* G1 vs. G5 Dunnett's multiple
1235 comparisons test $p=0.87$, *ns*, **(L)** and for H-OM test sessions; Repeated measures ANOVA,
1236 $p=0.32$, *ns.* G1 vs. G5 Dunnett's multiple comparisons test $p=0.98$, *ns,* not significant. **(M)** AUC
1237 quantifications of the reward approach only evoked changes in GCaMP6s activity across the
1238 different test sessions for correct 'C' and premature 'P' trials. Two-tailed paired t-tests. H-SMS-C
1239 vs. H-SMS-P: ***$p<0.001$. S-SMS-C vs. S-SMS-P: *$p<0.05$. H-NCal-C vs. H-NCal-P: $p=0.80$, ns.
1240 H-Suc-C vs. H-Suc-P: $p=0.12$, ns. H-H_2O-C vs. H-H_2O-P $p=0.69$, ns. H-OM-C vs. H-OM-P
1241 $p=0.75$, ns. Two-tailed unpaired t-tests. H-SMS-C vs. H-OM-C *$p<0.05$. H-SMS-P vs. H-OM-P
1242 **$p<0.01$. **(N)** AUC quantifications of the reward delivery and feeding bouts-evoked changes in
1243 GCaMP6s activity across the different test sessions. Two-tailed paired t-tests. H-SMS baseline

1244 (base) vs. H-SMS: ***$p<0.001$. base vs. S-SMS: **$p<0.01$. base vs. H-NCal: ****$p<0.0001$. Base

1245 vs. H-Suc: ***$p<0.001$. base vs. H-H_2O: $p=0.50$, ns. base vs. H-OM: $p=0.60$, ns, not significant.

1246

1247

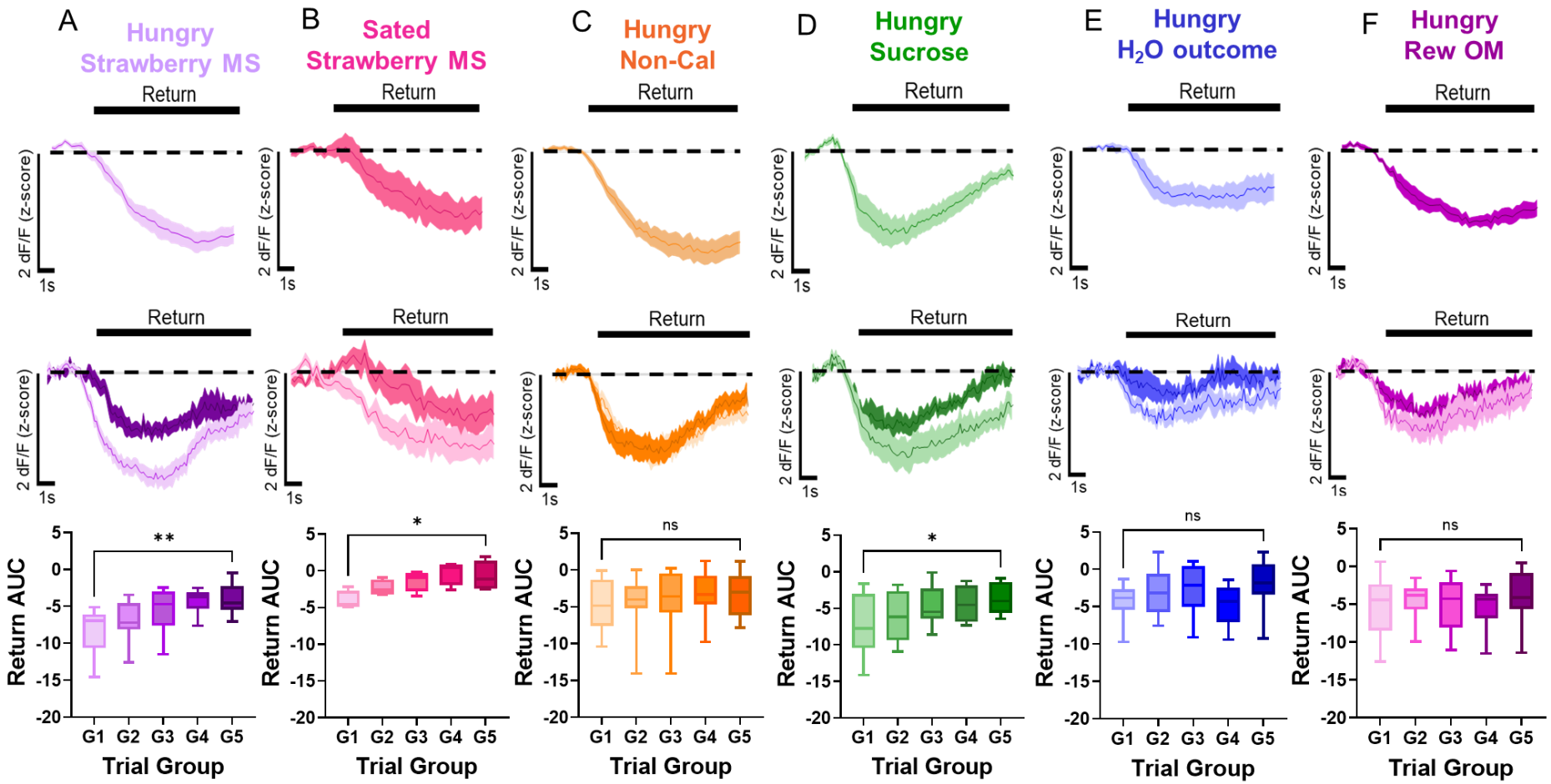
A
Hungry
Strawberry MS
B
Sated
Strawberry MS
C
Hungry
Non-Cal
D
Hungry
Sucrose
E
Hungry
H2O outcome
F
Hungry
Rew OM
Return
2 dF/F (z-score)
1s
Return AUC
Trial Group
G1 G2 G3 G4 G5
**
*
ns
*
ns
ns

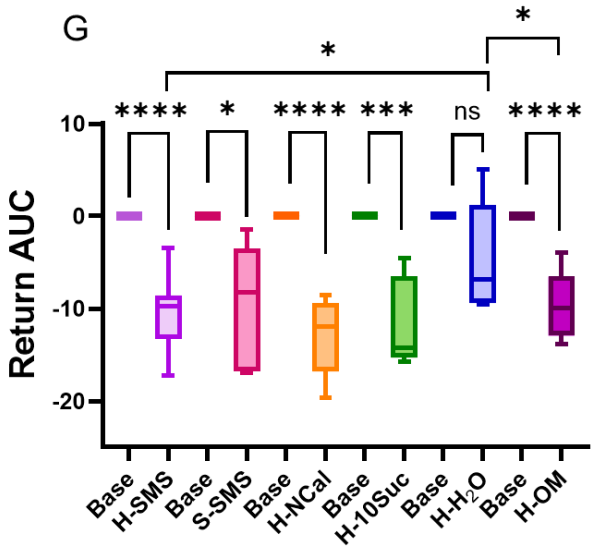
G
Return AUC
****
*
****
***
ns
****
*
*
Base
H-SMS
Base
S-SMS
Base
H-NCal
Base
H-10Suc
Base
H-H2O
Base
H-OM

Figure 5

1248 **Figure 5. PVT^{D2+} neuronal activity during return is modulated by outcome and outcome**
1249 **expectation.**

1250 **(A-F)** Average GCaMP6s responses from PVT^{D2+} neurons (top), comparisons between early
1251 'G1' and late 'G5' trials (middle) and AUC quantifications across trial groups (bottom) during
1252 return to trigger zone for the **(A)** H-SMS test sessions; Repeated measures ANOVA,
1253 ****$p<0.0001$. G1 vs. G5 Dunnett's multiple comparisons test **$p<0.01$, **(B)** for S-SMS test
1254 sessions; Repeated measures ANOVA, **$p<0.01$. G1 vs. G5 Dunnett's multiple comparisons
1255 test *$p<0.05$, **(C)** for H-NCal test sessions; Repeated measures ANOVA, $^{\#}p=0.06$, *ns.* G1 vs. G5
1256 Dunnett's multiple comparisons test $^{\#}p=0.06$, *ns*, **(D)** for H-Suc test sessions; Repeated
1257 measures ANOVA, *$p<0.05$. G1 vs. G5 Dunnett's multiple comparisons test *$p<0.05$, **(E)** for H-
1258 H_2O test sessions; Repeated measures ANOVA, $^{\#}p=0.05$, *ns.* G1 vs. G5 Dunnett's multiple
1259 comparisons test $^{\#}p=0.08$, *ns*, **(F)** and for H-OM test sessions; Repeated measures ANOVA,
1260 $p=0.41$, *ns.* G1 vs. G5 Dunnett's multiple comparisons test $p=0.63$, *ns,* not significant. **(G)** AUC
1261 quantifications of the return-evoked changes in GCaMP6s activity across the different test
1262 sessions. Two-tailed paired t-tests. H-SMS baseline (base) vs. H-SMS: ****$p<0.0001$. base vs.
1263 S-SMS: *$p<0.05$. base vs. H-NCal: ****$p<0.0001$. Base vs. H-Suc: ***$p<0.001$. base vs. H-H_2O:
1264 $p=0.08$, ns. base vs. H-OM: ****$p<0.0001$. Two-tailed unpaired t-tests. H-SMS vs H-H_2O:
1265 *$p<0.05$. H-H_2O vs. H-OM: *$p<0.05$.

1266

1267

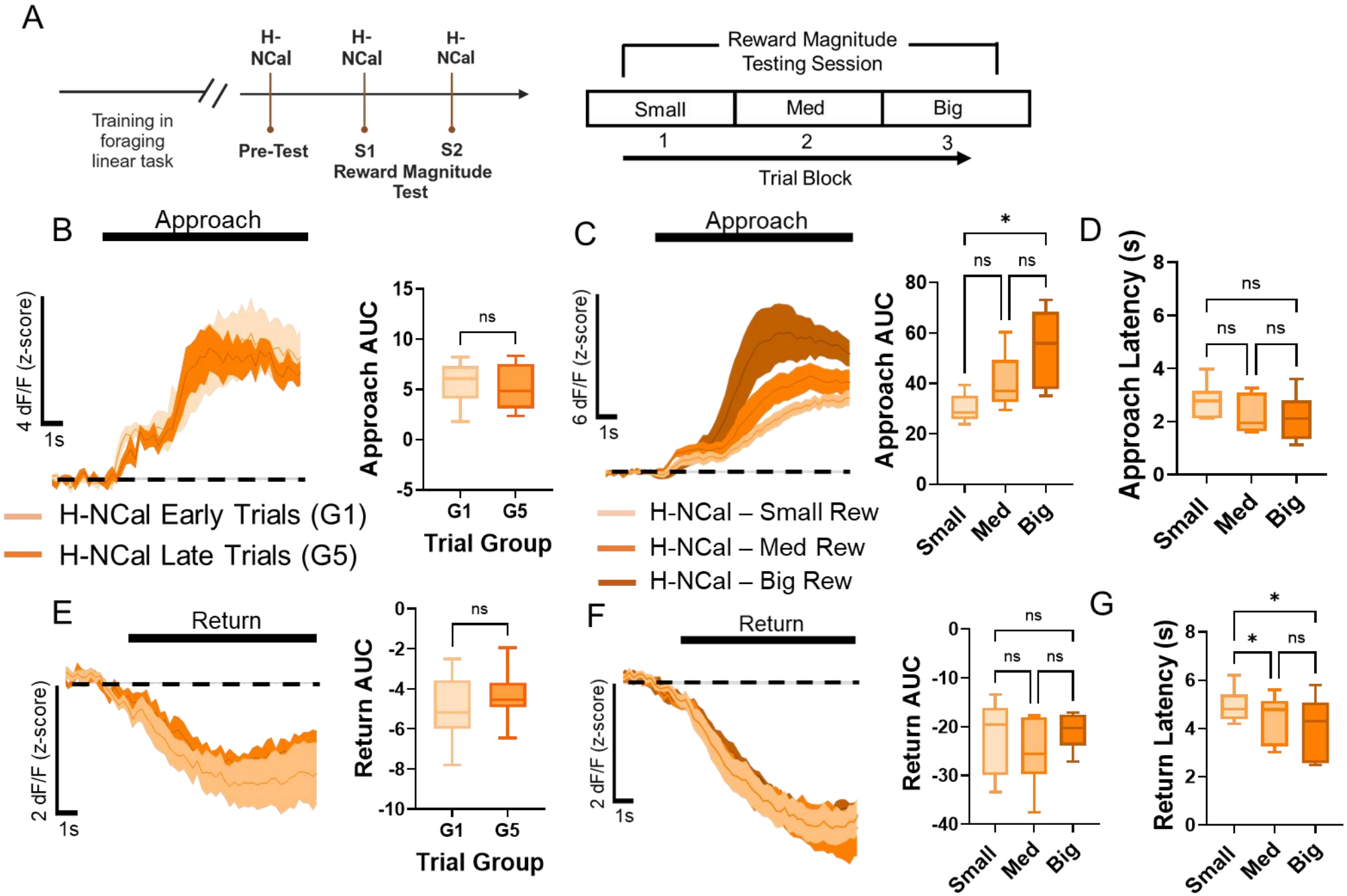
A
H-NCal
H-NCal
H-NCal
Training in foraging linear task
Pre-Test
S1
S2
Reward Magnitude Test
Reward Magnitude Testing Session
Small
Med
Big
1
2
3
Trial Block
B
Approach
4 dF/F (z-score)
1s
Approach AUC
ns
G1
G5
Trial Group
H-NCal Early Trials (G1)
H-NCal Late Trials (G5)
C
Approach
6 dF/F (z-score)
1s
Approach AUC
ns
ns
*
Small
Med
Big
H-NCal – Small Rew
H-NCal – Med Rew
H-NCal – Big Rew
D
Approach Latency (s)
ns
ns
ns
Small
Med
Big
E
Return
2 dF/F (z-score)
1s
Return AUC
ns
G1
G5
Trial Group
F
Return
2 dF/F (z-score)
1s
G
Return AUC
ns
ns
ns
Small
Med
Big
Return Latency (s)
*
*
ns
Small
Med
Big

Figure 6

1268 **Figure 6. PVT^{D2+} neurons detect changes in reward magnitude.**

1269 **(A)** *Left:* Schematic of the timeline for the test of reward magnitude changes. *Right:* Schematics
1270 of the reward magnitude test session showing that each session was divided into 3 trials blocks
1271 in which mice received non-cal reward of different magnitudes: small (1µl), medium (3µl), and
1272 big (6µl). **(B)** *Left:* Average GCaMP6s responses from PVT^{D2+} neurons during the pre-test with
1273 a non-caloric reward. *Right:* AUC quantification showing comparisons between ramping activity
1274 during reward approach for early (G1) and late (G5) trials. Two-tailed paired t-test. G1 vs. G5,
1275 *p=0.48.* **(C)** *Left:* Average GCaMP6s responses from PVT^{D2+} neurons to the different reward
1276 amounts during approach. *Right:* AUC quantification showing comparisons between ramping
1277 activity during reward approach for the small, medium, and big reward. Repeated measures
1278 ANOVA, *$p<0.05$. Small vs. Medium: Tukey's multiple comparisons test $p=0.27$. Small vs. Big:
1279 Tukey's multiple comparisons test *$p<0.05$. Medium vs. Big: Tukey's multiple comparisons test
1280 $p=0.16$ *ns*, not significant. **(D)** Latencies to reach the reward zone for the small, medium and big
1281 rewards. Repeated measures ANOVA, $^{\#}p=0.06$. Small vs. Medium: Tukey's multiple
1282 comparisons test $^{\#}p=0.06$. Small vs. Big: Tukey's multiple comparisons test $p=0.18$. Medium vs.
1283 Big: Tukey's multiple comparisons test $p=0.38$ *ns*, not significant. **(E)** *Left:* Average GCaMP6s
1284 responses from PVT^{D2+} neurons during return of the pre-test session. *Right:* AUC quantification
1285 showing comparisons between ramping activity during reward approach for early (G1) and late
1286 (G5) trials. Two-tailed paired t-test. G1 vs. G5, *p=0.21.* **(F)** *Left:* Average GCaMP6s responses
1287 from PVT^{D2+} neurons during return. *Right:* AUC quantification showing comparisons between
1288 return activity for the small, medium, and big reward. Repeated measures ANOVA, *p=0.47.*
1289 Small vs. Medium: Tukey's multiple comparisons test $p=0.59$. Small vs. Big: Tukey's multiple
1290 comparisons test $p=0.96$. Medium vs. Big: Tukey's multiple comparisons test $p=0.48$ *ns*, not
1291 significant. **(G)** Latencies for the return for the small, medium and big rewards. Repeated
1292 measures ANOVA, *$p<0.05$. Small vs. Medium: Tukey's multiple comparisons test *$p<0.05$.

Small vs. Big: Tukey's multiple comparisons test *$p<0.05$. Medium vs. Big: Tukey's multiple comparisons test $p=0.33$ *ns*, not significant.

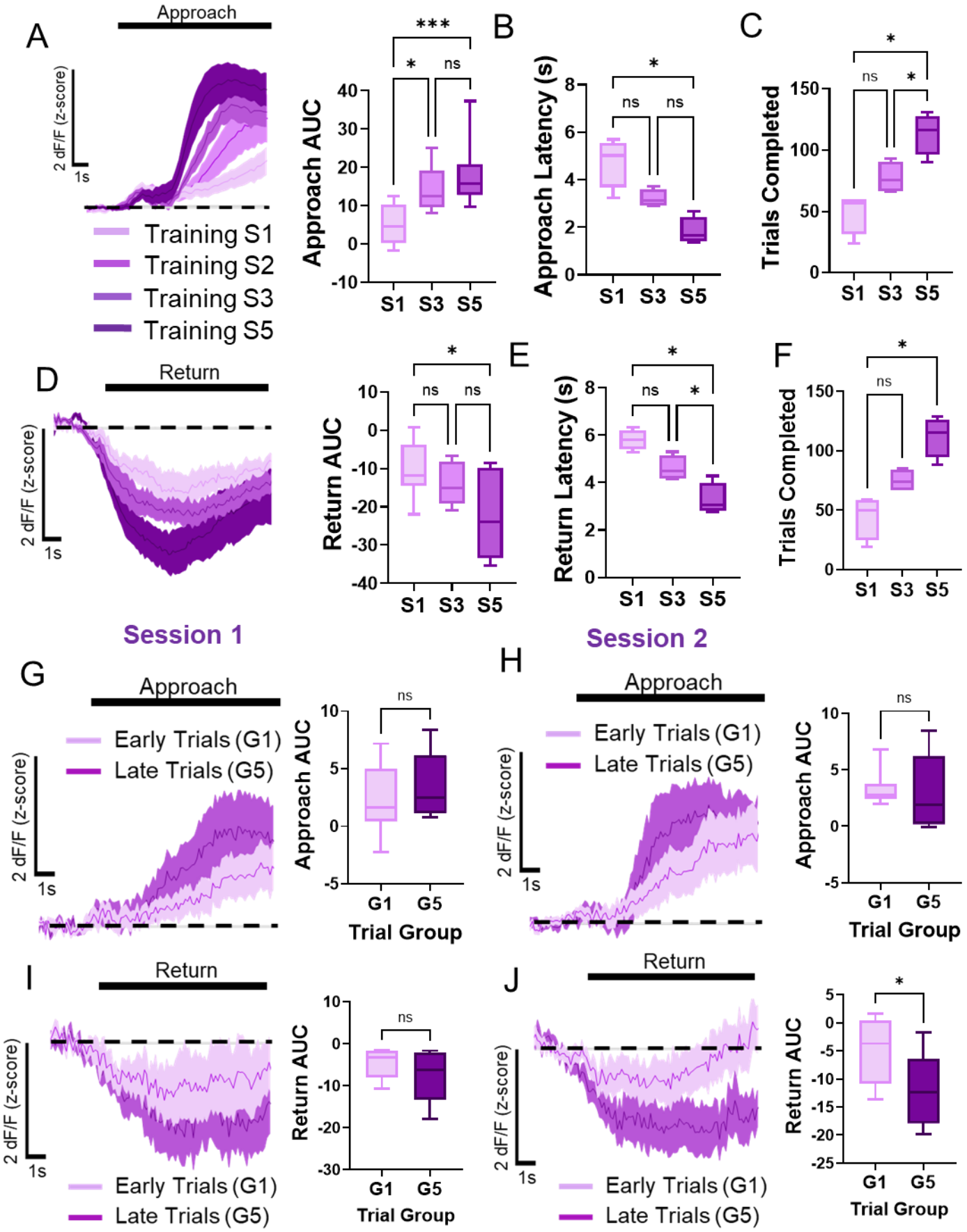
A
Approach
2 dF/F (z-score)
1s
Training S1
Training S2
Training S3
Training S5
Approach AUC
***
*
ns
S1
S3
S5
B
Approach Latency (s)
C
Trials Completed
D
Return
Return AUC
E
Return Latency (s)
F
Session 1
Session 2
G
Early Trials (G1)
Late Trials (G5)
G1
G5
Trial Group
H
I
J

Figure 7

Figure 7. PVT^{D2+} neuronal responses during approach and return emerge from the learning of cue–outcome associations.

(A) Average GCaMP6s responses from PVT^{D2+} neurons and AUC quantification showing comparisons between ramping activity during reward approach for the first 'S1', second 'S2', third 'S3' and fifth 'S5' training session in our linear foraging task. Repeated measures ANOVA, ****p<0.001.* S1 vs. S3 Tukey's multiple comparisons test **p<0.05*. S1 vs. S5 Tukey's multiple comparisons test ****p<0.001*. S3 vs. S5 Tukey's multiple comparisons test *p=0.60* ns, not significant. **(B)** Latencies to reach the reward zone for training sessions 'S1', 'S3' and 'S5'. Repeated measures ANOVA, ***p<0.01.* S1 vs. S3 Tukey's multiple comparisons test $^{\#}$*p=0.06*. S1 vs. S5 Tukey's multiple comparisons test ***p<0.01*. S3 vs. S5 Tukey's multiple comparisons test *p=0.08* ns, not significant. **(C)** Correct approach trials performed during training sessions 'S1', 'S3' and 'S5'. Repeated measures ANOVA, **p<0.05.* S1 vs. S3 Tukey's multiple comparisons test *p=0.25, ns,* not significant. S1 vs. S5 Tukey's multiple comparisons test **p<0.05*. S3 vs. S5 Tukey's multiple comparisons test **p<0.05.* **(D)** Average GCaMP6s responses from PVT^{D2+} neurons and AUC quantification during return to trigger zone for the first 'S1', second 'S3', and fifth 'S5' training session in our linear foraging task. Repeated measures ANOVA, **p<0.05.* S1 vs. S3 Tukey's multiple comparisons test *p=0.54* ns. S1 vs. S5 Tukey's multiple comparisons test **p<0.01*. S3 vs. S5 Tukey's multiple comparisons test *p=0.14* ns, not significant. **(E)** Latencies to return to the trigger zone for training sessions 'S1', 'S3' and 'S5'. Repeated measures ANOVA, **p<0.05.* S1 vs. S3 Tukey's multiple comparisons test *p=0.15*. S1 vs. S5 Tukey's multiple comparisons test **p<0.05*. S3 vs. S5 Tukey's multiple comparisons test **p<0.05*. **(F)** Total return trials performed during training sessions 'S1', 'S3' and 'S5'. Repeated measures ANOVA, **p<0.05.* S1 vs. S3 Tukey's multiple comparisons test *p=0.25, ns,* not significant. S1 vs. S5 Tukey's multiple comparisons test **p<0.05*. S3 vs. S5 Tukey's multiple comparisons test **p<0.05.* **(G)** Average GCaMP6s responses and AUC quantification from

PVT^{D2+} neurons comparing reward approach between early ‘G1’ and late ‘G5’ trials for the first training session. Two-tailed paired t-test. G1 vs. G5, *p=0.95.* **(H)** Average GCaMP6s responses and AUC quantification from PVT^{D2+} neurons comparing reward approach between early ‘G1’ and late ‘G5’ trials for the second training session. Two-tailed paired t-test. G1 vs. G5, *p=0.92.* **(I)** Average GCaMP6s responses from PVT^{D2+} neurons comparing return to trigger zone between early ‘G1’ and late ‘G5’ trials for the first training session. Two-tailed paired t-test. G1 vs. G5, *p=0.09.* **(J)** Average GCaMP6s responses from PVT^{D2+} neurons comparing return to trigger zone between early ‘G1’ and late ‘G5’ trials for the second training session. Two-tailed paired t-tests. G1 vs. G5, *p=0.41.*

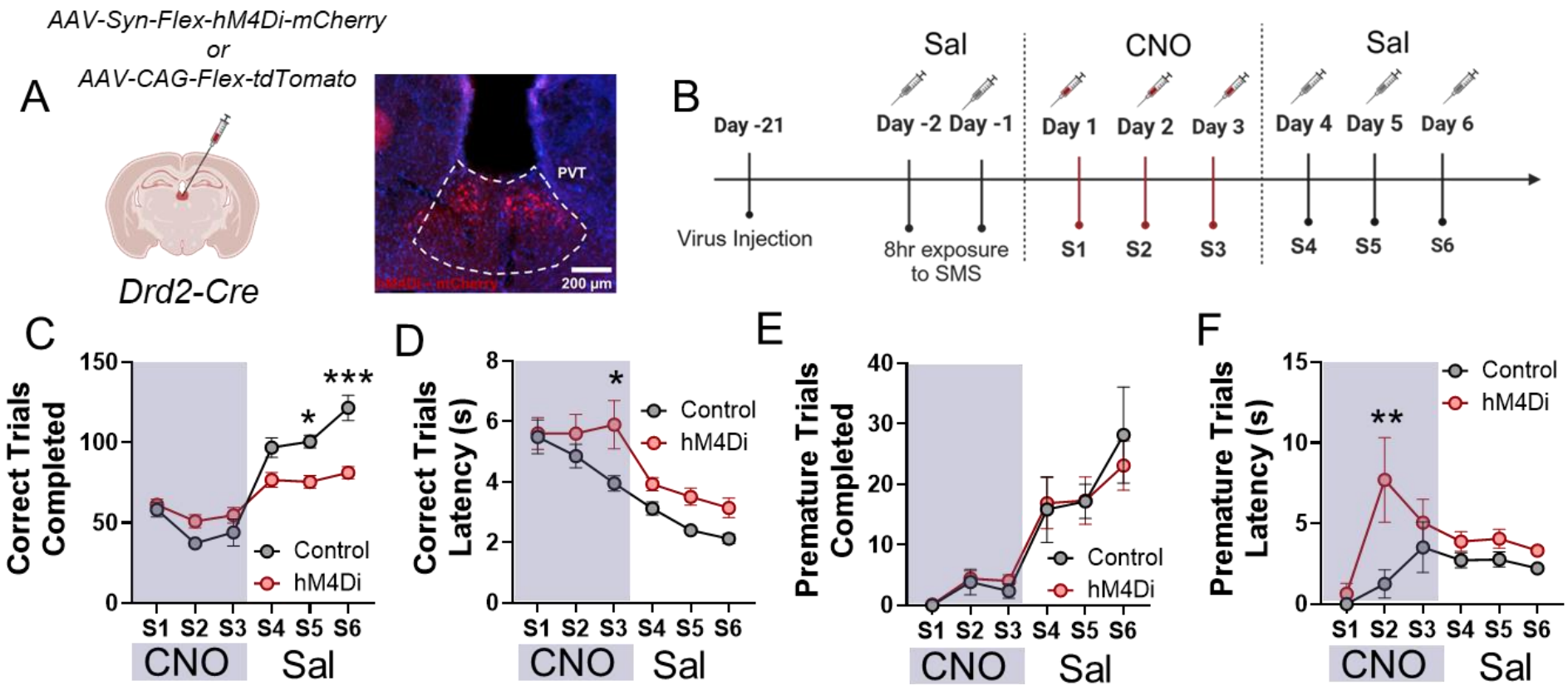
A
AAV-Syn-Flex-hM4Di-mCherry
or
AAV-CAG-Flex-tdTomato
Drd2-Cre
PVT
200 µm
B
Sal
CNO
Sal
Day -21
Day -2
Day -1
Day 1
Day 2
Day 3
Day 4
Day 5
Day 6
Virus Injection
8hr exposure to SMS
S1
S2
S3
S4
S5
S6
C
Correct Trials Completed
Control
hM4Di
CNO
Sal
D
Correct Trials Latency (s)
E
Premature Trials Completed
F
Premature Trials Latency (s)

Figure 8

Figure 8. Chronic PVT^{D2+} neuronal inhibition impairs performance in the foraging tasks.

(A) Right: Schematic of the stereotaxic injections for targeting D2+ neurons in the PVT. Left: Representative image from a Drd2-Cre mouse expressing hM4Di-mcherry in the PVT. **(B)** Schematics of the timeline for the chemogenetic inhibition of PVT^{D2+} neurons. **(C)** Quantification of correct trials completed for hM4Di and Controls groups. Two-way ANOVA, Effect of test session ****$p<0.0001$. Effect of viral group ***$p<0.001$. Interaction $p=0.0001$. Šídák's multiple comparisons test: (S5) control vs. hM4Di, *$p<0.05$; (S6) control vs. hM4Di, ***$p<0.001$. **(D)** Quantification of latency to approach during correct trials for hM4Di and Controls groups. Two-way ANOVA, Effect of test session ****$p<0.0001$. Effect of viral group ***$p<0.001$; Interaction $p=0.50$, *ns*. Šídák's multiple comparisons test: (S3) control vs. hM4Di, *$p<0.05$. **(C)** Quantification of premature trials completed for hM4Di and Controls groups. Two-way ANOVA, Effect of test session ****$p<0.0001$. Effect of viral group $p=0.91$,*ns.* Interaction $p=0.86$, *ns*. **(D)** Quantification of latency to approach during premature trials for hM4Di and Controls groups. Two-way ANOVA, Effect of test session *$p<0.05$. Effect of viral group **$p<0.01$. Interaction $p=0.24$, *ns*. Šídák's multiple comparisons test: (S2) control vs. hM4Di, **$p<0.01$.

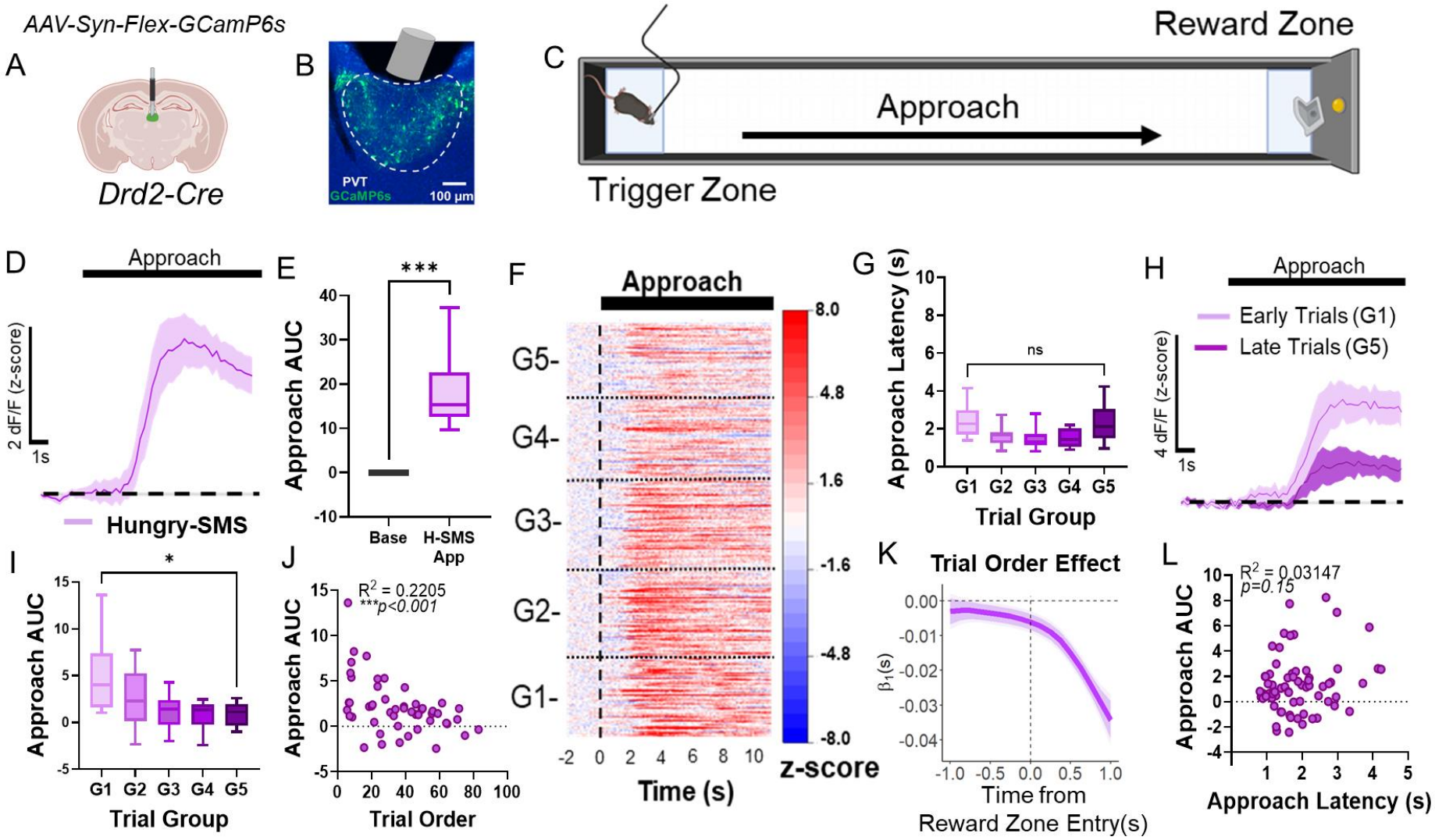

Supplementary Figure 1

Supplementary Figure 1. PVT^{D2+} neurons sense and track hunger states.

(A) Schematic of the stereotaxic injections and optical fiber implantation for targeting D2+ neurons in the PVT. **(B)** Representative image from a Drd2-Cre mouse expressing GCaMP6s in the PVT. **(C)** Schematics depicting the foraging-like reward-seeking task. **(D)** Average GCaMP6s responses from PVT^{D2+} neurons showing ramping activity during reward approach. **(E)** Quantification of the approach-evoked changes in GCaMP6s fluorescence in PVT^{D2+} neurons. Area under the curve (AUC), n = 705 trials from 5 mice. Comparisons between baseline (base) and approach (H-SMS app); two-tailed paired t-test, ****p<0.001*. **(F)** Heatmap showing excitatory reward approach responses from PVT^{D2+} neurons, time-locked to approach onset, sorted by trial order, and binned into 5 'trial group blocks' (G1 – G5). **(G)** Latencies to reach the reward zone across 'trial group blocks' (G1 – G5). Repeated measures ANOVA, ***p<0.01*; G1 vs. G5 Dunnett's multiple comparisons test *p=0.98*; ns, not significant. **(H)** Average GCaMP6s responses from PVT^{D2+} neurons comparing reward approach between early 'G1' and late 'G5' trials within the test sessions. **(I)** AUC quantification of the reward approach-evoked changes in GCaMP6s activity across trial group blocks. Repeated measures ANOVA, ***p<0.001*. G1 vs. G5 Dunnett's multiple comparisons test **p<0.05*.
(J) Correlation between the AUC of the reward approach-evoked changes in GCaMP6s activity and trial order within a test session. **(K)** FLMM coefficient estimates plots of the approach trial order effect and statistical significance at each trial time-point for the photometric responses of PVT^{D2+} neurons for reward zone entry. The plot shows a negative association between PVT^{D2+} GCaMP6s responses and trial order before and after reward zone entry. **(L)** No correlation between the AUC of the reward approach-evoked changes in GCaMP6s activity and approach latency within a test session.

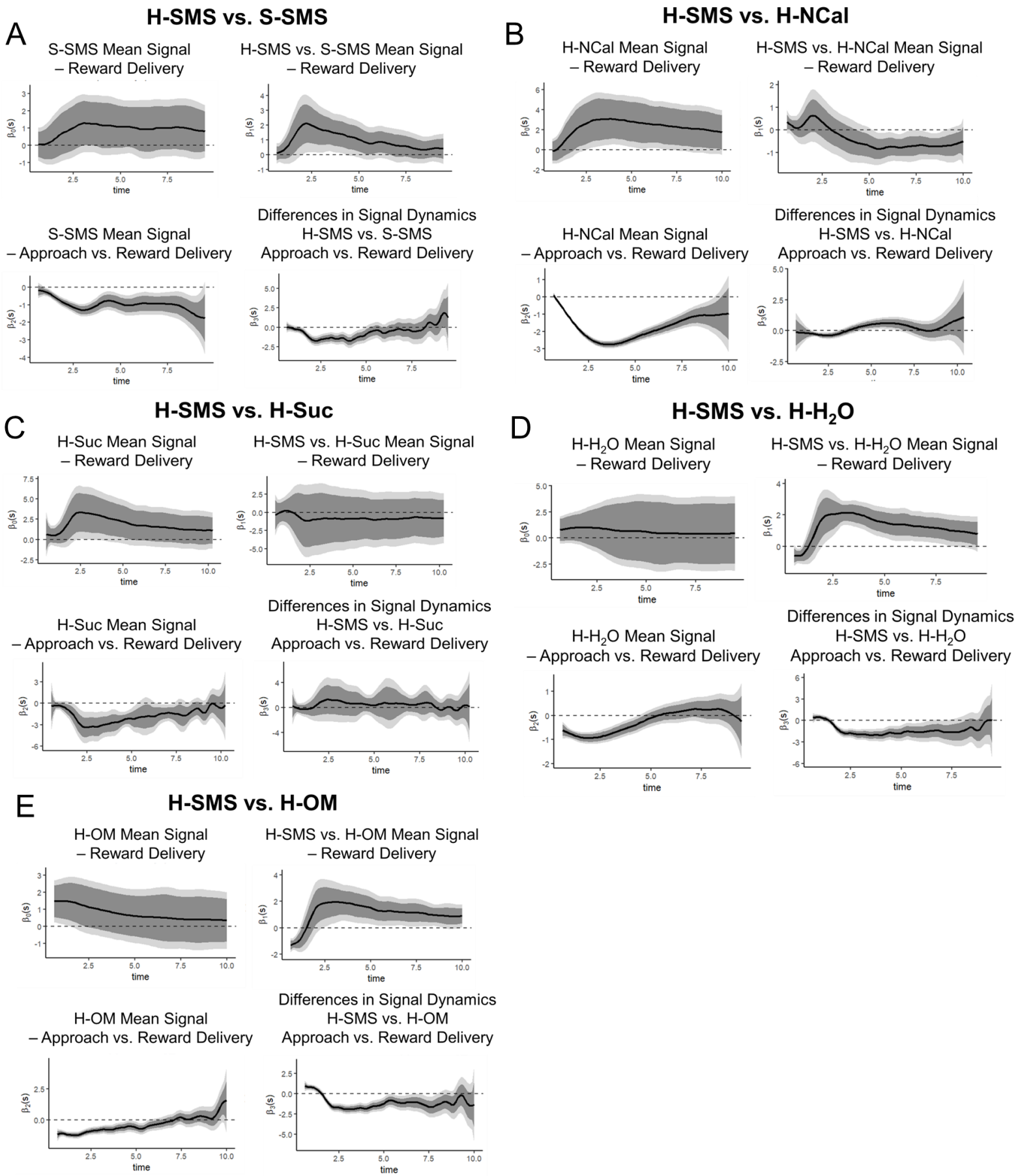

Supplementary Figure 2

1373 **Supplementary Figure 2. Concurrent FLMM model of between conditions comparisons.**

1374 **(A-E)** FLMM coefficient estimates plots and statistical significance at each trial time-point for the
1375 mean changes in photometric responses of PVT^{D2+} neurons during approach and reward delivery
1376 for the between outcomes comparisons (i.e., H-SMS vs. 'other outcome'). Each plot shows the
1377 four beta coefficients that result from these comparisons. *Top left* - $\beta_0(s)$: shows the mean signal
1378 when the mouse received the 'other outcome'. *Top right* - $\beta_1(s)$: shows the mean difference in
1379 signal between H-SMS and the 'other outcome' during reward delivery. *Bottom left* - $\beta_2(s)$: shows
1380 the mean difference between approach and outcome delivery for the 'other outcome'. *Bottom right*
1381 - $\beta_3(s)$: shows the difference of differences, capturing the additional effect on signal when the
1382 mouse is approaching the 'other outcome' that is not already captured by $\beta_0(s)+\beta_1(s)+\beta_2(s)$. As
1383 such, $\beta_3(s)$ captures the interaction effect between behavioral state (approaching vs. reward
1384 delivery) and outcome condition (H-SMS vs. 'other outcome').

1385 **(A)** Beta coefficients for the comparisons of the H-SMS and S-SMS conditions. $\beta_0(s)$: shows that
1386 during reward delivery in the S-SMS condition, the mean signal is not significantly modulated.
1387 $\beta_1(s)$: shows that during reward delivery, the mean signal is significantly higher for H-SMS
1388 compared to S-SMS conditions. $\beta_2(s)$: shows that the mean signal during approach is significantly
1389 lower than the mean signal during reward delivery for the S-SMS condition. $\beta_3(s)$: shows a
1390 significant negative interaction effect between behavioral states (approaching vs. receiving) and
1391 conditions (H-SMS vs. S-SMS), showing that the mean changes in photometric responses are
1392 larger during the outcome delivery than during approach. Specifically, there are larger mean
1393 changes during H-SMS than in the S-SMS conditions.

1394 **(B)** Beta coefficients for the comparisons of the H-SMS and H-NCal conditions. $\beta_0(s)$: shows that
1395 during reward delivery in the H-NCal condition, the mean signal is significantly positively
1396 modulated by the NCal rewards. $\beta_1(s)$: shows that during reward delivery, the mean signal is

significantly lower for H-SMS compared to H-NCal conditions. $\beta_2(s)$: shows that the mean signal during approach is significantly lower than the signal during reward delivery for the H-NCal condition. $\beta_3(s)$: shows a significant negative interaction early in the trial, followed by positive interaction effects later in the trial and during reward delivery. This indicates that the differences in neural activity during the early approach are significantly lower, but later in the trial and during reward consumption, they are significantly higher in the NCal than in the H-SMS conditions.

(C) Beta coefficients for the comparisons of the H-SMS and H-Suc conditions. $\beta_0(s)$: shows that during reward delivery in the H-Suc condition, the mean signal is positively modulated by the Suc rewards, however, this was not significant. $\beta_1(s)$: shows that during reward delivery, the mean signal for H-SMS is not significantly different than the signal during the H-Suc conditions. $\beta_2(s)$: shows that the mean signal during approach is significantly lower than the signal during reward delivery for the H-Suc condition. $\beta_3(s)$: shows no significant interaction effects between behavioral states (approaching vs. receiving) and conditions (H-SMS vs. H-Suc).

(D) Beta coefficients for the comparisons of the H-SMS and H-H_2O conditions. $\beta_0(s)$: shows that during reward delivery in the H-H_2O condition, the mean signal is not significantly modulated. $\beta_1(s)$: shows that during reward delivery, the mean signal is significantly higher for H-SMS compared to H-H_2O conditions. $\beta_2(s)$: shows that the mean signal during approach is significantly lower than the signal during outcome delivery for the H-H_2O condition. $\beta_3(s)$: shows a significant negative interaction effect between behavioral states (approaching vs. receiving) and conditions (H-SMS vs. H-H_2O), showing that the mean changes in photometric responses are larger during the outcome delivery than during approach. Specifically, there are larger mean changes during H-SMS than in the H-H_2O conditions.

(E) Beta coefficients for the comparisons of the H-SMS and H-OM conditions. $\beta_0(s)$: shows that during reward delivery in the H-OM condition, the mean signal is positively modulated initially by

the omission of the rewards, but the signal quickly goes down over time. $\beta_1(s)$: shows that during reward delivery, the mean signal is significantly higher for H-SMS compared to H-OM conditions. $\beta_2(s)$: shows that the mean signal during approach is significantly lower than the signal during outcome delivery for the H-OM condition. $\beta_3(s)$: shows a significant positive interaction early in the trial, followed by negative interaction effects later in the trial and during reward delivery. This indicates that the differences in neural activity during the early approach are higher, but later in the trial and during reward consumption, they are lower in H-OM than in the H-SMS conditions.

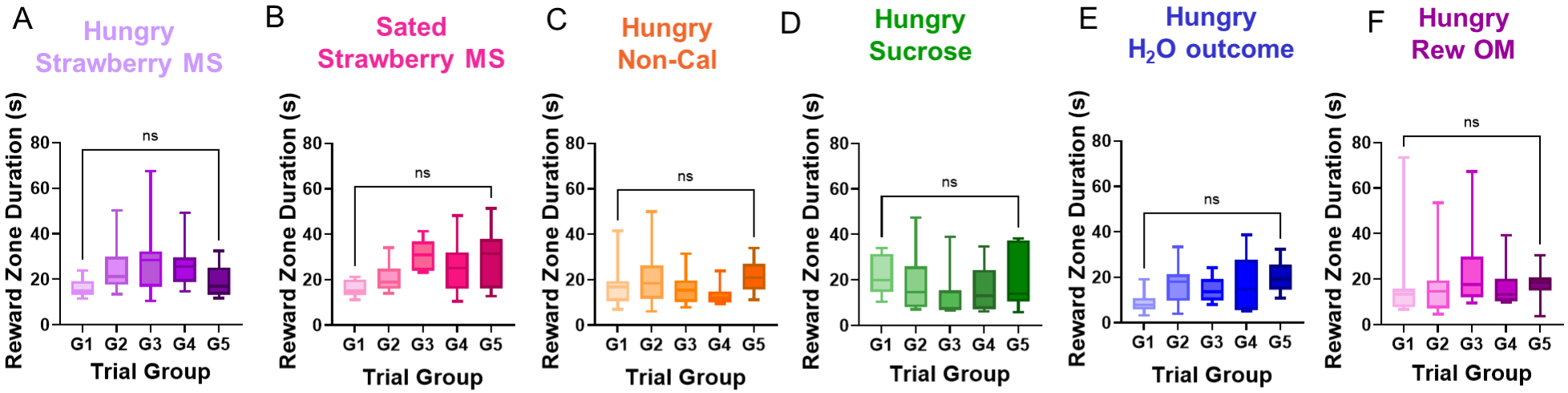

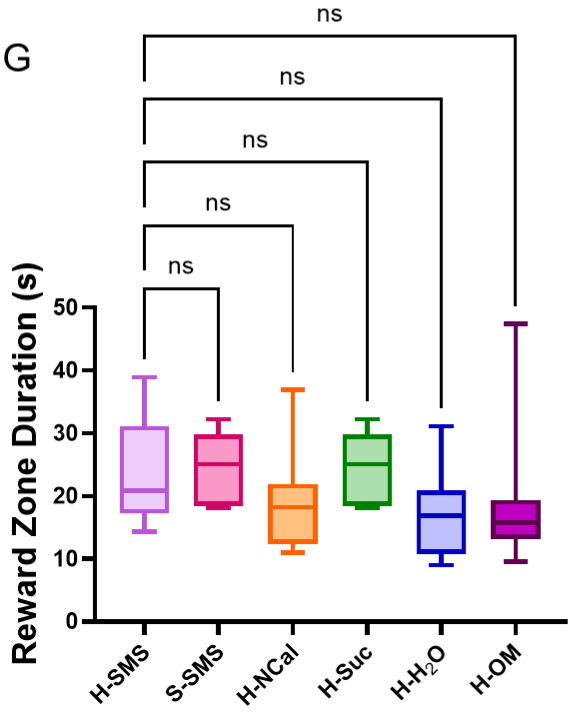

Supplementary Figure 3

1428 **Supplementary Figure 3. Time spent in the reward zone after reward delivery does not**
1429 **differ across outcome groups or trial groups.**
1430 **(A-F)** Quantifications of time spent in the reward zone after reward delivery and prior to return
1431 across trial groups for the **(A)** H-SMS test sessions; Repeated measures ANOVA, *p=0.07, ns.* G1
1432 vs. G5 Dunnett's multiple comparisons test *p=0.52, ns*. **(B)** S-SMS test sessions; Repeated
1433 measures ANOVA, *p=0.11, ns.* G1 vs. G5 Dunnett's multiple comparisons test *p=0.07, ns*. **(C)** H-
1434 NCal test sessions; Repeated measures ANOVA, *p=0.16.* G1 vs. G5 Dunnett's multiple
1435 comparisons test *p=0.77, ns*. **(D)** H-Suc test sessions; Repeated measures ANOVA, *p=0.44.* G1
1436 vs. G5 Dunnett's multiple comparisons test *p=0.95*. **(E)** H-H_2O test sessions; Repeated measures
1437 ANOVA, *p=0.11, ns.* G1 vs. G5 Dunnett's multiple comparisons test *p=0.06, ns*. **(F)** H-OM test
1438 sessions; Repeated measures ANOVA, *p=0.51, ns.* G1 vs. G5 Dunnett's multiple comparisons
1439 test *p=0.99, ns*. **(G)** Quantifications of time spent in the reward zone after reward delivery and
1440 prior to return across outcome groups. Repeated measures ANOVA, *p=0.26, ns.* H-SMS vs. S-
1441 SMS Dunnett's multiple comparisons test *p=0.99, ns*, not significant. H-SMS vs. H-NCal Dunnett's
1442 multiple comparisons test *p=0.63, ns*, not significant. H-SMS vs. H-Suc Dunnett's multiple
1443 comparisons test *p=0.99, ns*, not significant. H-SMS vs. H-H_2O Dunnett's multiple comparisons
1444 test *p=0.32, ns*, not significant. H-SMS vs. H-OM Dunnett's multiple comparisons test *p=0.49, ns*,
1445 not significant.
1446

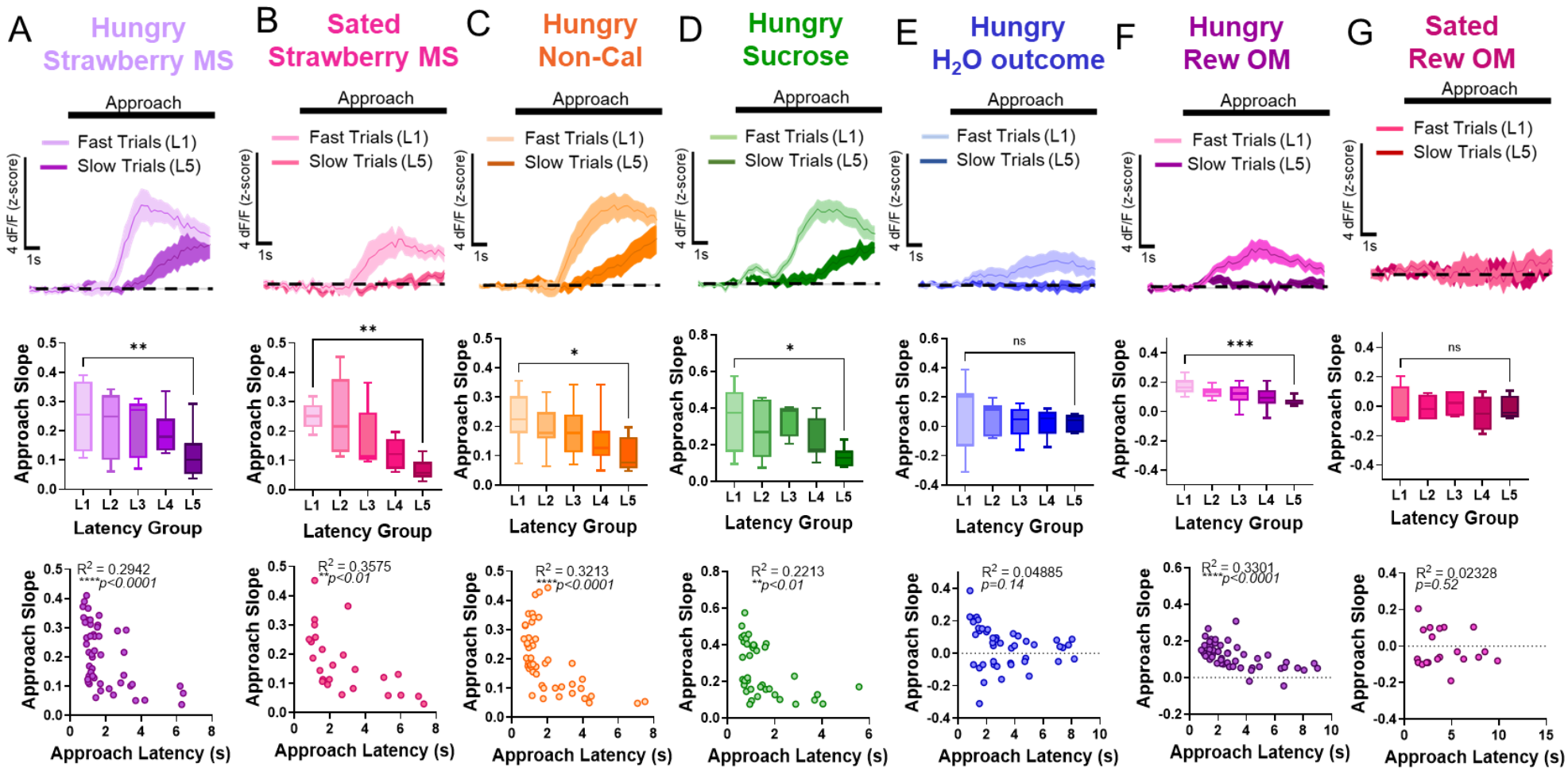

Supplementary Figure 4

1447 **Supplementary Figure 4. Motivational states are associated with PVT^{D2+} neuronal**
1448 **responses across different conditions.**

1449 **(A-G)** Average GCaMP6s responses from PVT^{D2+} neurons comparing between fast 'L1' and slow
1450 'L5' trials (top). AUC quantifications across latency groups during approach (middle). Correlations
1451 between the approach slope and the latency to approach (bottom) for the **(A)** H-SMS test
1452 sessions; Repeated measures ANOVA, $^{**}p<0.01$. L1 vs. L5 Dunnett's multiple comparisons test
1453 $^{**}p<0.01$. **(B)** S-SMS test sessions; Repeated measures ANOVA, $^{\#}p=0.06$. L1 vs. L5 Dunnett's
1454 multiple comparisons test $^{**}p<0.01$. **(C)** H-NCal test sessions; Repeated measures ANOVA,
1455 $^{*}p<0.05$. L1 vs. L5 Dunnett's multiple comparisons test $^{*}p<0.05$. **(D)** H-Suc test sessions;
1456 Repeated measures ANOVA, $^{**}p<0.01$. L1 vs. L5 Dunnett's multiple comparisons test $^{*}p<0.05$.
1457 **(E)** H-H_2O test sessions; Repeated measures ANOVA, *p=0.62, ns.* L1 vs. L5 Dunnett's multiple
1458 comparisons test *p=0.95, ns*. **(F)** H-OM test sessions; Repeated measures ANOVA, $^{**}p<0.01$. L1
1459 vs. L5 Dunnett's multiple comparisons test $^{***}p<0.001$. **(G)** S-OM test sessions; Repeated
1460 measures ANOVA, *p=0.57, ns.* L1 vs. L5 Dunnett's multiple comparisons test *p=0.99, ns*, not
1461 significant.

1462